Contrib Mineral Petrol (2006) 151: 558–581
DOI 10.1007/s00410-006-0066-7

ORIGINAL PAPER

R. M. Flowers · S. A. Bowring · M. L. Williams

Timescales and significance of high-pressure, high-temperature metamorphism and mafic dike anatexis, Snowbird tectonic zone, Canada

Received: 1 August 2005 / Accepted: 18 January 2006 / Published online: 22 March 2006

Abstract New geochronological, isotopic and geochemical data for a spectacular swarm of deep crustal migmatitic mafic dikes offer important insight into processes operative during 1.9 Ga high pressure, high temperature metamorphism along the Snowbird tectonic zone in northern Saskatchewan. High-precision U–Pb zircon dates reveal anatexis of Chipman mafic dikes at 1,896.2 ± 0.3 Ma during syntectonic and synmetamorphic intrusion at conditions of 1.0–1.2 GPa, >750°C. U–Pb zircon dates of 1,894–1,891 Ma for cross-cutting pegmatites place a lower bound on major metamorphism and deformation at the currently exposed crustal levels. The persistence of elevated temperatures for ~14 m.y. following peak conditions is implied by younger U–Pb titanite dates, and by Sm–Nd whole rock isotopic data that suggest the derivation of the pegmatites by melting of a mafic source. Limited melting of the host felsic gneiss at 1.9 Ga despite high temperature is consistent with evidence for their previous dehydration by granulite facies metamorphism in the Archean. Spatial heterogeneity in patterns of mafic dike and tonalitic gneiss anatexis can be attributed to lateral peak temperature and compositional variability. We correlate 1,896 Ma Chipman mafic dike emplacement and metamorphism with substantial 1.9 Ga mafic magmatism over a minimum along-strike extent of 1,200 km of the Snowbird tectonic zone. This suggests a significant, continent-wide period of asthenospheric upwelling that induced incipient continental rifting. Extension was subsequently terminated by hinterland contraction associated with Trans-Hudson accretion and orogenesis. Little activity in the lower crust for ca. 650 m.y. prior to Proterozoic metamorphism and mafic magmatism implies an extended interval of cratonic stability that was disrupted at 1.9 Ga. This episode of destabilization contrasts with the record of long-term stability in most preserved cratons, and is important for understanding the lithospheric characteristics and tectonic circumstances that control the destruction or survival of continents.

Communicated by T. L. Grove

R. M. Flowers (✉) · S. A. Bowring
Department of Earth, Atmospheric and Planetary Sciences, Massachusetts Institute of Technology, 02139 Cambridge, Massachusetts, USA
E-mail: rflowers@gps.caltech.edu

M. L. Williams
Department of Geosciences, University of Massachusetts, 01003 Amherst, Massachusetts, USA

Present address: R. M. Flowers
Division of Geological and Planetary Sciences, California Institute of Technology, MS 100-23, Pasadena, CA 91125, USA

Introduction

Rare exposures of lower continental crust offer the best opportunity to directly scrutinize this generally inaccessible level of orogenic systems. As models for the rheological, metamorphic and melting behavior of the deep crust are developed, it becomes increasingly critical to test these ideas through careful study of exhumed lower crustal rocks. In particular, constraining the nature, intensity and duration of tectonometamorphic events in these exposures is key to deciphering the complexities of, and interactions between, deep crustal mafic magmatism, silicic melt generation and segregation, metamorphic reactions, and deformation. The interplay of these processes in the lower crust can have a profound impact on the behavior of the entire crustal column during transfer of mass, heat and stress through the system. In addition, the deep crust contains a signature of activity in the underlying lithospheric and asthenospheric mantle. Thus, unraveling the record of processes preserved in lower crustal exposures can simultaneously yield important insights into both crustal and mantle dynamics.

The East Lake Athabasca region, along the Snowbird tectonic zone in the western Canadian Shield, contains a vast (>20,000 km^2) well-preserved exposure of

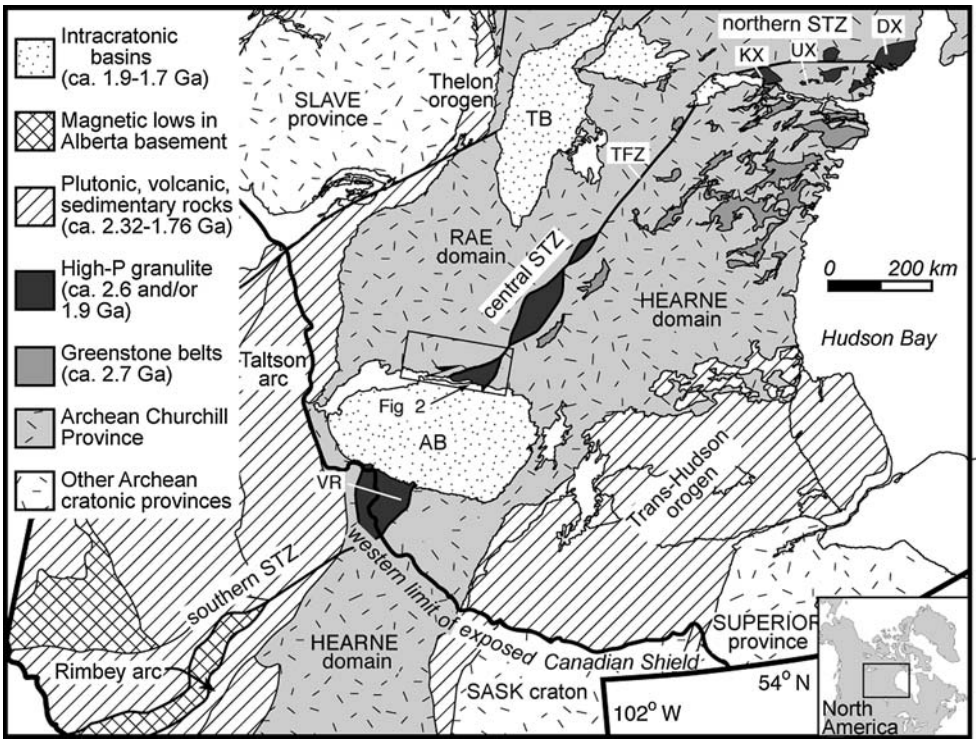

Fig. 1 Geological map of the western Canadian shield showing major tectonic features. *AB* Athabasca basin, *DX* Daly Bay Complex, *KX* Kramanituar Complex, *STZ* Snowbird tectonic zone, *TB* Thelon Basin, *TFZ* Tulemalu Fault Zone, *UX* Uvauk Complex, *VR* Virgin River shear zone. The *rectangle* shows the East Lake Athabasca region enlarged in Fig. 2

high-pressure granulites (1.0 to >1.5 GPa) that provides an exceptional opportunity to study lower crustal processes (Fig. 1). In particular, the Chipman mafic dike swarm, exposed within this tract of rocks, preserves a spectacular snapshot of a dynamic deep crustal environment during high temperature metamorphism (Figs. 2, 3). During emplacement, the mafic dikes were metamorphosed, heterogeneously deformed, and partially melted at 1.0–1.2 GPa, >750°C to yield segregations of tonalitic and trondhjemitic melt (Williams et al. 1995). We use new high-precision U–Pb isotope dilution-thermal ionization mass spectrometry (ID-TIMS)

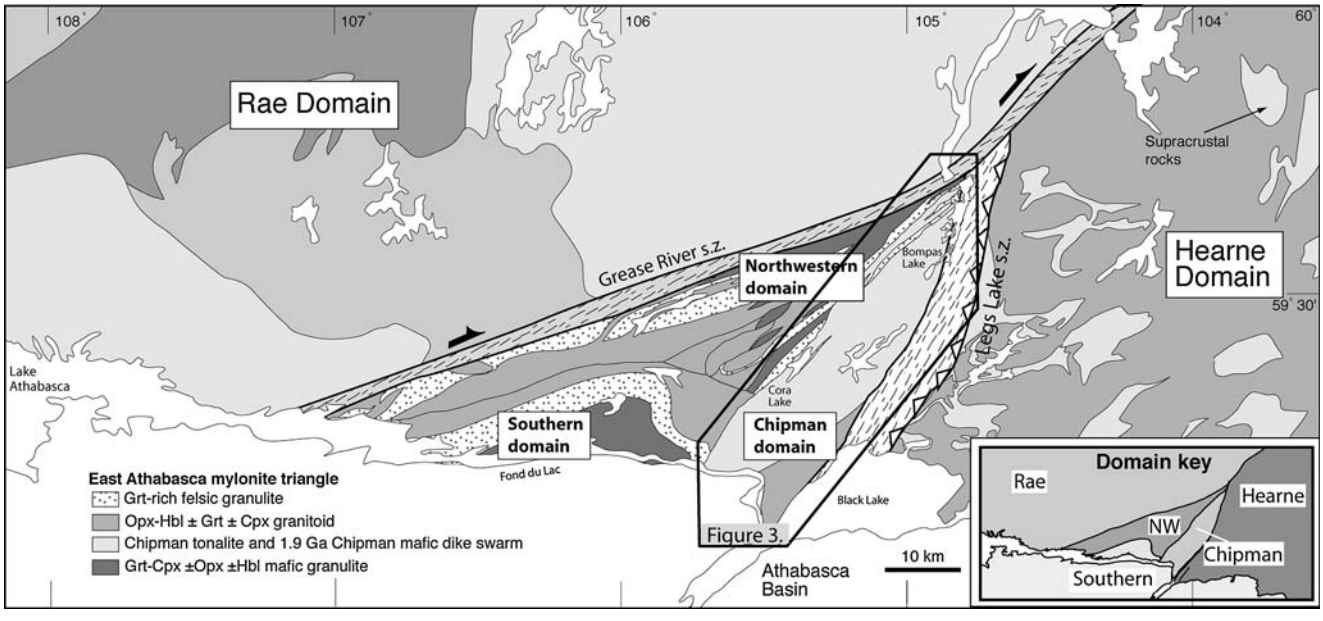

Fig. 2 Geological map of the East Lake Athabasca region, northern Saskatchewan. The *box outline* shows the location of the study area enlarged in Fig. 3

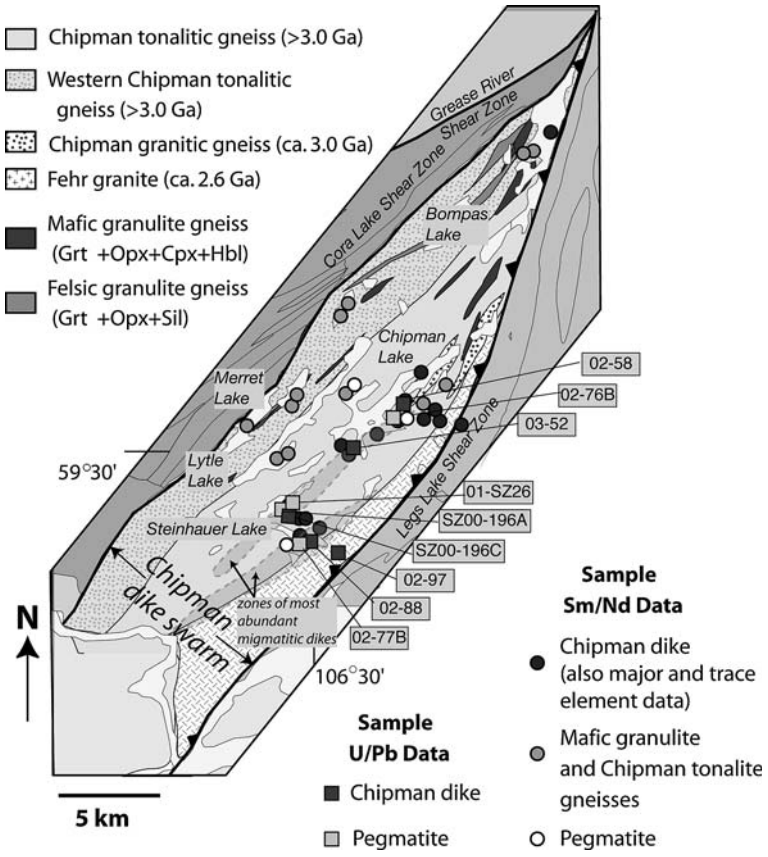

Fig. 3 Geological map of the Chipman domain with sample locations

geochronological data, Sm–Nd isotopic systematics, geochemistry, and field observations to constrain the duration of high pressure–high temperature metamorphism, anatexis, and deformation in this region, unravel the evolution of the thermal regime during this event, and assess the geodynamic significance of this intense episode of deep crustal magmatism and metamorphism. Our results highlight the exceptional value of deep crustal exposures like the East Lake Athabasca region for understanding the nature, behavior, and response of the lower crust during the evolution, stabilization, and reactivation of continents.

Geological setting

The western Churchill Province of the Canadian Shield is an extensive region of Archean crust bounded by the Thelon orogen (2.02–1.90 Ga) to the northwest and the Trans-Hudson orogen (1.85–1.80 Ga) to the southeast (Fig. 1). The Snowbird tectonic zone, a 2,800 km long NE trending gravity and magnetic anomaly, has been defined as the boundary separating the Rae and Hearne cratons of the western Churchill Province (Goodacre et al. 1987; Hoffman 1988). This dramatic geophysical feature has alternatively been interpreted as a Paleoproterozoic intercontinental suture (Hoffman 1988; Ross et al. 1995, 2000), an Archean intracontinental strike-slip shear zone (Hanmer 1994, 1997; Hanmer et al. 1995a, b), and a Paleoproterozoic intracontinental transform (Lewry and Sibbald 1980). The central segment of the Snowbird tectonic zone is characterized by an anastomosing internal geometry that recently has been attributed to the interaction of Proterozoic intracontinental thrust and strike-slip shear zones (Mahan and Williams 2005). In this region, the East Lake Athabasca region in northern Saskatchewan contains an enormous tract of high-grade rocks (1.0 to ≥1.5 GPa, >750°C), composed of several disparate domains, spanning the width of this fundamental structure (Fig. 2).

The East Lake Athabasca region includes granulite facies rocks of the East Athabasca mylonite triangle along the trace of the Snowbird tectonic zone, deep crustal rocks of the Rae domain to the west, and middle to upper crustal rocks of the Hearne domain to the east (e.g., Hanmer 1997). To the south the region is covered by sedimentary rocks of the Athabasca basin. The East Athabasca mylonite triangle is divided into three distinct lithotectonic domains: (1) the Chipman domain dominated by the heterogeneous >3.0 Ga Chipman tonalite and the extensive Chipman mafic dike swarm recording metamorphism and melting at 1.0–1.2 GPa and 750–850°C (Williams et al. 1995), (2) the northwestern domain composed of ca. 2.6 Ga mafic to felsic plutonic rocks, including granitic rocks

interpreted to have been intruded and metamorphosed at 1.0 GPa (Williams et al. 2000), and (3) the southern domain consisting of felsic and mafic granulites and minor eclogite with peak metamorphic conditions as high as ≥1.5 GPa and 900–1,000°C (Snoeyenbos et al. 1995; Baldwin et al. 2003, 2004). Southern domain eclogite facies metamorphism has recently been interpreted to have occurred at 1904.0 ± 0.3 Ma (Baldwin et al. 2004). Metamorphic studies in the Rae domain at Neil Bay and Wholdaia Lake document granulite-facies conditions of ~0.8 GPa, 900°C at ca. 1.9 Ga (Kopf 1999; Krikorian 2002). The Legs Lake shear zone (LLSZ) along the eastern margin of the Chipman domain juxtaposes granulite facies rocks of the East Athabasca mylonite triangle with lower pressure (~0.5 GPa, 600–700°C) rocks of the Hearne domain, and is associated with regional exhumation of the deep crustal rocks at ca. 1,850–1,800 Ma (Mahan et al. 2003; Mahan and Williams 2005).

Chipman mafic dike metamorphic assemblages and field relationships

The Chipman mafic dike swarm, originally named by Macdonald (1980), is exposed across the width of the Chipman domain and is truncated laterally by domain-bounding shear zones (Fig. 3). The >3.0 Ga variably deformed Chipman tonalite gneisses, containing inclusions of anorthosite, peridotite, and mafic and felsic granulites, compose the dominant host unit in the domain. The more homogeneous ca. 2.6 Ga Fehr granite occurs on the eastern margin of the domain. Chipman dikes vary in abundance across the span of the swarm, range in width from less than one to tens of meters, and locally comprise 60–100% of the exposure. In the western part of the Chipman domain dikes are locally abundant, but do not intrude the adjacent northwestern domain. Near the western boundary of the domain, the dikes are locally deformed by mylonites of the Cora Lake shear zone, a structure interpreted to truncate western exposures of the dike swarm. The northeast striking Chipman dikes are deformed by the more northerly striking LLSZ on the east side of the Chipman domain (Fig. 3). Dikes decrease in abundance from the Chipman tonalite into rocks of the Fehr granite, and are increasingly scarce eastward in rocks deformed by the LLSZ.

The Chipman dikes can be texturally and mineralogically subdivided into four major groups: (1) migmatitic Grt + Hbl + Pl dikes, (2) non-migmatitic Grt + Cpx + Hbl + Pl dikes, (3) non-migmatitic Hbl + Pl dikes, and (4) phenocrystic or phyric Hbl + Pl ± Grt ± Cpx dikes. Accessory phases include variable amounts of titanite, ilmenite, rutile and zircon. Migmatitic dikes typically are characterized by centimeter-scale garnet and associated zircon-bearing quartz and plagioclase leucosomes in a hornblende and plagioclase matrix (Fig. 4a). Leucosomes occur as tails in strain shadows adjacent to garnet crystals, and, with increasing melt volumes, as discrete leucosomal segregations in pods and veins (Fig. 4b). Some migmatitic dikes show an internal textural layering parallel to the dike contacts. In partly migmatized dikes, the migmatitic components typically occur along dike margins. In non-migmatitic garnet-bearing dikes, textures range from fine-grained Grt + Cpx spherical clumps in a Hbl + Pl matrix, to a homogeneous fine- to coarse-grained Grt + Cpx + Hbl + Pl matrix (Fig. 4c). Non-migmatitic Hbl + Pl dikes are typically homogeneous and medium to coarse grained. Phenocrystic to phyric dikes contain plagioclase crystals that range up to centimeter-scale in length. Non-migmatitic dikes lack zircon grains of significant size. Textures suggest that all dikes crystallized as Hbl + Pl rocks and were metamorphosed to produce the garnet-bearing assemblages. The remaining Hbl + Pl dikes either never reacted to form the garnet-bearing assemblage, or are retrogressed varieties of garnet-bearing dikes. Additional detailed descriptions of mineralogical assemblages and textures in the Chipman dikes, with particular focus on the migmatitic dikes, were provided in Williams et al. (1995). Thermobarometric estimates for migmatitic and non-migmatitic dikes using Grt + Hbl and Grt + Cpx thermometry and Grt + Hbl + Pl and Grt + Cpx + Pl barometry yielded conditions of 750–850°C and 1.0–1.2 GPa (Williams et al. 1995).

Migmatitic and non-migmatitic dikes differ in both their distribution and degree of strain. Migmatitic dikes occur in a 10–12 km wide corridor within the broader Chipman dike exposures. They are abundant in the Chipman tonalite in the southeastern part of the domain, are less common in the Fehr granite to the east, and were not observed in the western part of the domain. In contrast, non-migmatitic dikes are distributed across the entire domain. Migmatitic dikes always contain a moderately steep NE-striking fabric, and, in places, contain an earlier, shallower NW-striking fabric. These dikes are commonly boudinaged with leucocratic melt filling boudin necks, or may be folded with leucocratic melt tails either folded or defining the axial surface of the fold (Fig. 4d). In contrast, non-migmatitic dikes typically show less strain than migmatitic dikes, are commonly discordant to fabric in the host rocks (Fig. 4e), and may preserve original intrusive features such as apophyses into the host tonalite. The differing strain may owe to the inherently greater strength of dikes lacking leucosomes and/or later intrusion of non-migmatitic dikes that missed an earlier phase of deformation.

Documentation of the detailed spatial relationships of dismembered, folded, variably deformed, and cross-cutting dikes suggests their synmetamorphic and syntectonic emplacement at granulite facies conditions (Williams et al. 1995). For example, observations of dikes with straight leucocratic tails cutting dikes with folded leucocratic tails (see Williams et al. 1995, Fig. 7) are most simply explained by episodic or continuous

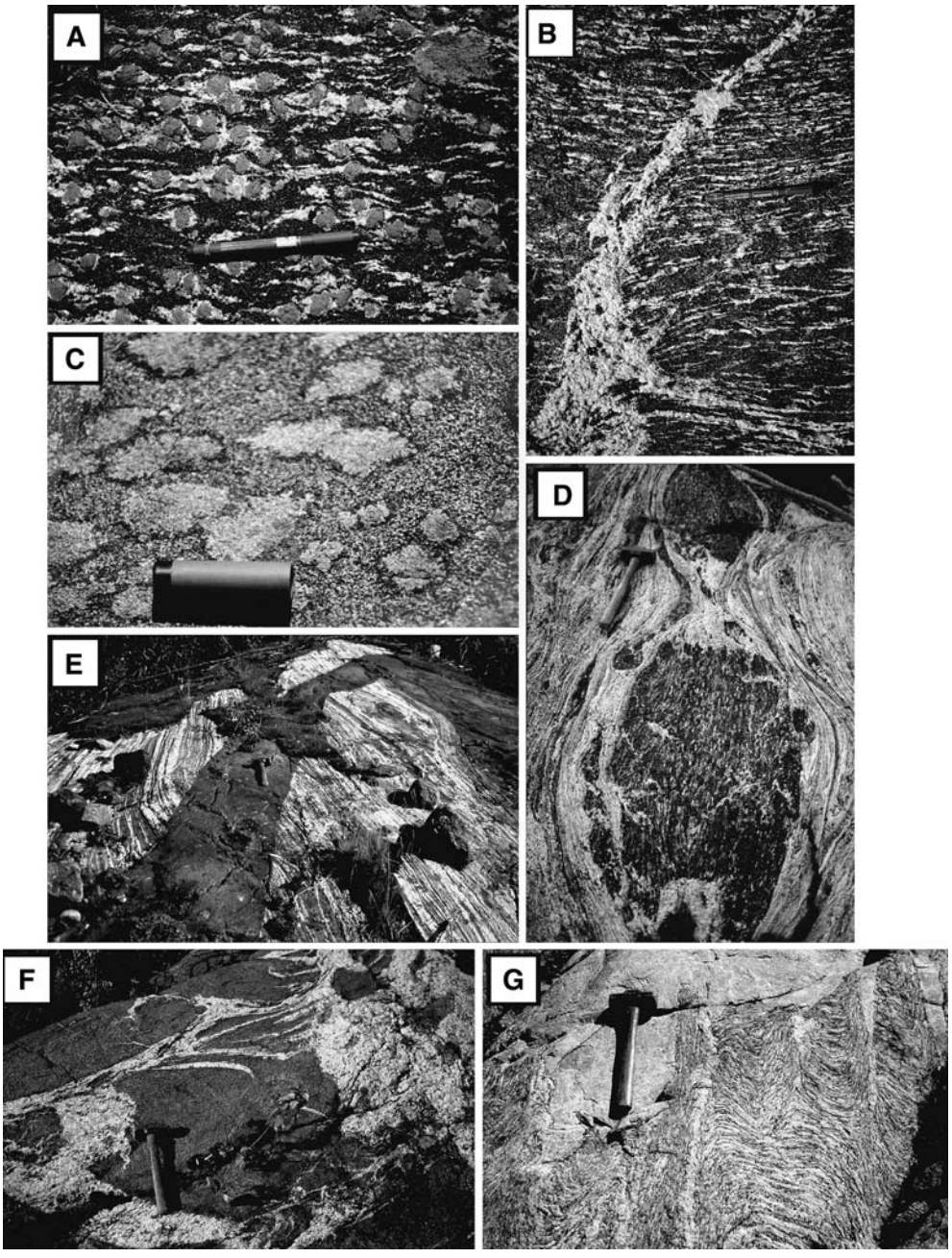

Fig. 4 Example Chipman mafic dike relationships and textures. **a** Migmatitic Grt + Hbl + Pl dike with large centimeter-scale garnets with associated leucosome tails. **b** Leucocratic segregation, 3–12 cm wide, in a migmatitic dike. **c** Non-migmatitic dike with several cm wide Grt + Cpx clumps in a Hbl + Pl matrix. **d** Boudins of a migmatitic dike. **e** Non-migmatitic garnet-bearing dike, ~1 m wide, discordantly cutting heterogeneous Chipman gneisses. **f** Pegmatite intruding mafic dike. **g** Inferred ca. 1.9 Ga melt in Fehr granite

migmatization of dikes during intrusion rather than a single discrete anatectic event that postdated their emplacement. Importantly, this interpretation implies that determination of the time of dike anatexis also constrains the date of dike intrusion. Although intrusion of multiple dike swarms of widely differing ages with more than one episode of dike migmatization cannot currently be excluded as a means of explaining the field relationships, this requires a significantly more complex geological history that is not supported by the data in this study.

Pegmatitic dikes and segregations intrude Chipman dikes of varying textures and metamorphic assemblages (Fig. 4f). Undeformed varieties provide the potential to impose a local lower temporal bound on major magmatism and deformation in the domain. With the exception of the pegmatites and migmatitic dike leucosomes, limited melting during mafic dike intrusion is indicated by field relationships. Centimeter scale felsic bands, segregations, and leucosomal material in the hornblende-bearing Chipman tonalite are inferred to be coeval with Chipman dike intrusion based on structural and lithological relationships. In the biotite-bearing Fehr granite, more abundant felsic veins, sometimes defining a crenulation, are either directly or indirectly associated with mafic dikes and provide the most convincing field evidence for melting of host felsic rocks during dike emplacement (Fig. 4g). However, these felsic

veins have not been dated owing to their lack of zircon grains.

Whole rock geochemistry

Sixteen samples of Chipman dikes, representing the full spectrum of observed textural variation, were analyzed for major and trace elements by XRF and ICPMS at Activation Laboratories, respectively. Data are reported in Table 1. Data were acquired to evaluate the nature of the dike magma source and to assess the importance of compositional factors for dike anatexis by establishing whether dike geochemistry can be linked with textural and mineralogical observations. These results supplement major element data previously obtained for nine Chipman dike samples (Williams et al. 1995). Migmatitic dikes were characterized by the greatest textural heterogeneity, and particular care was taken to process samples representative of the bulk composition.

The dikes contain SiO_2 ranging from 46.1 to 52.2% and MgO from 3.3 to 7.1%. Samples in this study are relatively high in iron (iron as $Fe_2O_3 = 13.5$ to 19.5%) and low in Al_2O_3 (11.5–15.5%), with the exception of two plagioclase rich phyric to phenocrystic dikes (Fig.5a). Normative calculations and projections into the ol-cpx-qtz and ol-pl-qtz ternary systems result in a distribution of data that plot into the qtz and plag fields, consistent with most dikes representing melt compositions rather than residues of fractional crystallization. Spider diagrams reveal high field strength element (HFSE) depletions and large ion lithophile element (LILE) enrichments (Fig. 5b). Rare earth element (REE) patterns are relatively flat, implying an absence of significant garnet in the source (La/Yb = 0.7–4.8). Generally, migmatitic dikes contain higher SiO_2, Fe_2O_3, Ta, Zr and Nb, and lower MgO and Al_2O_3, than non-migmatitic dikes (Fig. 5a). Four distinct REE patterns generally correlate with the four major textural and mineralogical groups (Fig. 5c): (1) migmatitic dikes contain the highest REE contents, (2) non-migmatitic garnet-bearing dikes are characterized by an array of lower REE contents, (3) non-migmatitic Hbl + Pl dikes are defined by somewhat flatter REE patterns than those in the garnet-bearing dikes, and (4) phenocrystic and phyric dikes contain the lowest REE contents and are characterized by negative Eu anomalies. The occurrence of Eu anomalies in the two plagioclase-rich dike samples is consistent with the involvement of plagioclase fractionation near their source or during emplacement. A distinct coarse-grained sample from the center of a non-migmatitic granulite dike (02-112) is characterized by a shallow positive REE slope, contains the highest analyzed Mg content suggestive of a more primitive composition, and is considered from field observations to be one of the latest intruded dikes.

Sm–Nd isotopic systematics

Analytical methods

Whole rock powders were produced using standard shatterbox procedures. Sample powders (100–200 mg) were spiked with a mixed ^{149}Sm–^{150}Nd tracer, completely dissolved in HF–HNO_3 in Teflon pressure vessels at 220°C for 5 days, converted to 6 M HCl at 180°C for 24 h, then repeatedly fluxed in 6 M HCl at 120°C. The REE were separated from solution using cation exchange chemistry, followed by usage of LN-spec resin to isolate Sm and Nd. All analyses were carried out on the MIT Isoprobe-T mass spectrometer. Sm was loaded onto single Ta filaments with 1 M H_3PO_4 and analyzed as metal ions in multicollector static mode. Nd was loaded on triple Re filaments with 0.1 M H_3PO_4 and analyzed as metal ions in dynamic multicollector mode. Sm–Nd results and details regarding isotopic ratio corrections are provided in Table 2.

Analytical results

Archean gneisses

Whole rock Sm–Nd isotopic systematics were determined for four Chipman tonalitic gneiss samples and ten mafic granulite gneisses to place constraints on the sources of the Chipman dikes and associated pegmatites. The Chipman tonalite samples display evolved Nd isotopic signatures, with time-integrated LREE enrichment, ε_{Nd} values at 3.0 Ga from −4.4 to −1.8, and depleted mantle model dates (T_{DM}) from 3.56 to 3.28 Ga (Fig. 6a). These data are consistent with Sm–Nd data previously acquired for three samples of Chipman tonalite characterized by ε_{Nd} values at 3.0 Ga from −6.0 to −2.9 (Hanmer 1994).

Five Grt + Cpx + Opx + Pl mafic granulites and five Opx + Pl mafic granulites, collected from lenses in the Chipman tonalite in the western and northern parts of the Chipman domain, were selected for analysis. Previous data indicate metamorphism of these mafic granulite lenses at 2.55 Ga (Flowers 2005), with likely intrusion at ca. 2.6 Ga coincident with major magmatism in the region. Nine of ten mafic granulite samples are characterized by time-integrated LREE enrichment. One mafic granulite (03-228A) reflects time-integrated LREE depletion. The ε_{Nd} values at 2.6 Ga range from −7.29 to +2.72, with T_{DM} from 3.91 to 2.91 Ga (Fig. 6a). Our data show a correlation between ε_{Nd} values at 2.6 Ga and SiO_2 content, consistent with the assimilation of felsic crustal material characterized by more evolved Nd isotopic signatures during the generation and emplacement of the mafic granulite protolith (Fig. 6b). The mafic granulite with time-integrated LREE depletion is among the samples with the lowest

Table 1 Major and trace element data for Chipman mafic dikes

Sample:	Migmatitic Grt + Hbl + Pl dikes			Non-migmatitic Grt + CPx + Hbl + Pl dikes						Grt-bearing dikes with possible leucosomes		Non-migmatitic Hbl + Pl dikes			Phenocrystic or phyric dikes	
	O2-125	O2-58	99B-15	O2-112	SZ00-182A	SZ00-182B	SZ00-196D	O2-171C	SZ00-201A	O2-171B	SZ00-186A	01M123C	O2-120B	O2-123B	SZ00-200A	O2-172
SiO2	52.2	51.1	51.7	51.0	51.3	50.5	50.6	53.1	50.9	52.2	49.9	50.6	46.1	48.3	49.6	47.9
Al2O3	12.0	11.5	12.7	13.9	13.2	15.5	13.6	13.1	14.7	13.1	13.3	13.2	13.3	13.1	17.3	21.8
Fe2O3	17.5	19.5	16.2	13.5	16.2	13.3	15.7	15.5	14.5	15.6	16.9	15.5	18.9	16.6	10.0	5.7
MnO	0.2	0.3	0.3	0.2	0.2	0.2	0.2	0.2	0.2	0.2	0.3	0.2	0.3	0.2	0.2	0.1
MgO	4.4	3.3	4.9	7.1	5.3	6.0	6.0	5.2	5.6	5.2	5.7	5.8	5.6	5.4	7.1	5.7
CaO	9.0	7.8	8.9	11.5	9.6	10.5	10.4	9.3	9.3	9.0	9.9	9.7	9.5	9.6	11.8	14.5
Na2O	1.5	2.2	1.9	1.9	2.1	2.1	2.2	2.3	3.0	2.3	2.3	2.3	2.3	2.5	2.1	1.7
K2O	1.1	1.1	1.0	0.1	0.7	0.7	0.4	0.5	0.6	0.7	0.2	0.6	0.9	1.3	0.6	0.7
TiO2	1.9	2.5	1.8	0.7	1.5	1.2	1.5	1.2	1.2	1.1	1.4	1.4	2.4	1.8	0.6	0.3
P2O5	0.2	0.3	0.2	0.1	0.2	0.2	0.1	0.1	0.1	0.1	0.1	0.1	0.2	0.2	0.0	0.0
LOI	0.2	0.2	0.6	-0.4	-0.2	-0.1	-0.4	-0.1	-0.1	0.4	-0.3	0.6	0.5	0.8	1.2	1.7
Total	100.2	99.7	100.1	99.5	100.2	100.0	100.3	100.4	100.0	99.9	99.7	100.0	99.8	99.8	100.4	100.0
V	398	278	322	270	344	279	299	302	251	303	314	324	431	347	187	113
Cr	24	-20	46	119	90	158	113	43	26	64	24	65	95	107	214	233
Co	51	49	49	51	41	46	52	47	56	34	51	56	49	46	43	26
Ni	46	29	50	79	56	88	62	39	64	35	46	49	64	72	89	72
Cu	136	75	90	158	95	105	138	56	191	64	147	101	70	176	91	24
Zn	137	150	107	86	79	96	109	103	67	70	96	102	128	112	63	45
Ga	21	20	18	15	17	16	19	17	20	16	17	17	21	18	14	13
Ge	2	2	2	2	1	1	2	2	1	0	2	1	2	1	1	1
As	0	12	0	0	0	0	0	0	0	0	0	0	0	0	0	0
Rb	15	31	16	3	16	20	8	14	18	15	3	16	17	30	16	17
Sr	89	136	203	70	150	170	180	160	262	153	85	184	135	115	182	272
Y	35	45	25	19	30	24	22	23	22	21	31	22	39	33	11	6
Zr	165	211	115	38	123	102	90	85	74	75	84	89	140	115	35	20
Nb	11	13	14	5	7	6	6	5	4	4	6	9	9	8	3	3
Cs	0	0	1	0	0	1	0	0	1	0	0	0	0	1	2	2
Ba	142	287	169	25	231	225	136	176	219	158	27	119	181	160	87	84
La	16	27	18	2	17	13	10	11	10	8	6	11	11	13	3	2
Ce	37	59	37	5	37	28	22	23	21	20	15	22	27	23	7	4
Pr	5.4	7.9	5.1	0.8	4.7	3.8	3.2	3.3	2.8	2.6	2.3	3.0	4.1	3.6	1.0	0.6
Nd	24	34	22	4	21	17	15	14	12	12	11	14	19	17	5	3
Sm	6.2	8.5	5.2	1.5	5.3	4.2	3.9	3.6	3.3	3.2	3.6	3.6	5.8	4.9	1.4	0.8
Eu	1.9	2.4	1.7	0.7	1.6	1.3	1.3	1.2	1.2	1.1	1.2	1.2	1.9	1.6	0.6	0.4
Gd	6.1	8.2	4.9	2.3	5.9	4.3	4.1	3.7	3.5	3.9	4.2	3.9	6.4	5.6	1.7	0.9
Tb	1.1	1.4	0.8	0.5	1.0	0.8	0.7	0.7	0.6	0.7	0.9	0.7	1.2	1.0	0.3	0.2
Dy	6.8	8.6	4.9	3.4	6.0	4.7	4.4	4.4	4.1	4.1	5.8	4.0	7.4	6.6	2.1	1.1
Ho	1.3	1.7	1.0	0.8	1.2	0.9	0.9	0.9	0.8	0.9	1.2	0.8	1.5	1.3	0.4	0.2
Er	3.6	4.8	2.6	2.2	3.4	2.6	2.4	2.6	2.4	2.4	3.6	2.2	4.3	3.8	1.2	0.6
Tm	0.54	0.69	0.39	0.34	0.51	0.39	0.35	0.39	0.36	0.37	0.55	0.35	0.65	0.58	0.19	0.10
Yb	3.6	4.6	2.7	2.3	3.4	2.6	2.3	2.7	2.4	2.6	3.7	2.2	4.3	3.9	1.3	0.6
Lu	0.52	0.68	0.40	0.34	0.51	0.39	0.35	0.40	0.36	0.39	0.55	0.32	0.65	0.57	0.19	0.10

Table 1 (Contd.)

Sample:	Migmatitic Grt + Hbl + Pl dikes			Non-migmatitic Grt + CPx + Hbl + Pl dikes						Grt-bearing dikes with possible leucosomes		Non-migmatitic Hbl + Pl dikes			Phenocrystic or phyric dikes	
	O2-125	O2-58	99B-15	O2-112	SZ00-182A	SZ00-182B	SZ00-196D	O2-171C	SZ00-201A	O2-171B	SZ00-186A	01M123C	O2-120B	O2-123B	SZ00-200A	O2-172
Hf	4.9	6.1	3.5	1.2	3.7	3.0	2.7	2.7	2.3	2.4	2.6	2.5	4.3	3.6	1.1	0.7
Ta	0.81	1.07	1.08	0.00	0.42	0.32	0.37	0.25	0.20	0.25	0.32	0.32	0.51	0.42	0.00	0.00
W	2.44	0.00	0.00	0.00	1.68	0.00	0.00	0.00	0.00	0.00	0.00	0.00	0.00	0.00	0.00	0.00
Tl	0.14	0.20	0.15	0.00	0.00	0.11	0.00	0.11	0.00	0.00	0.00	0.00	0.00	0.20	0.00	0.14
Pb	0.00	8.22	0.00	0.00	0.00	0.00	0.00	0.00	0.00	0.00	0.00	0.00	0.00	5.28	0.00	5.47
Th	4.6	5.3	2.3	0.3	1.6	1.4	1.0	1.5	1.2	1.3	0.7	1.3	1.2	1.0	0.4	0.4
U	1.85	2.68	0.55	0.12	0.38	1.40	0.63	0.84	7.12	0.32	0.17	0.30	3.67	0.32	1.13	0.17
Recalculation of composition of protolith (Grove et al., 1992)																
Qtz	0.167	0.144	0.142	0.099	0.113	0.085	0.087	0.139	0.055	0.128	0.086	0.026	0.021	0.026	0.044	0.011
Plag	0.390	0.416	0.430	0.490	0.465	0.525	0.488	0.469	0.550	0.468	0.498	0.473	0.487	0.473	0.580	0.680
Oliv	0.170	0.173	0.172	0.175	0.177	0.169	0.178	0.172	0.171	0.175	0.189	0.173	0.204	0.173	0.157	0.096
Cpx	0.171	0.152	0.162	0.219	0.174	0.158	0.197	0.168	0.165	0.166	0.189	0.212	0.188	0.212	0.174	0.167
Or	0.071	0.073	0.065	0.006	0.046	0.044	0.027	0.034	0.040	0.045	0.015	0.085	0.061	0.085	0.036	0.041
Sp	0.027	0.036	0.025	0.010	0.021	0.017	0.020	0.016	0.016	0.016	0.020	0.026	0.034	0.026	0.008	0.004
Ap	0.004	0.006	0.004	0.001	0.004	0.003	0.003	0.002	0.002	0.002	0.002	0.004	0.004	0.004	0.001	0.001
Ternary Normalization																
Cpx	0.23	0.21	0.21	0.25	0.21	0.19	0.23	0.21	0.19	0.21	0.22	0.23	0.21	0.25	0.19	0.18
Pl	0.53	0.56	0.56	0.55	0.57	0.62	0.57	0.58	0.62	0.58	0.57	0.56	0.55	0.55	0.64	0.72
Ol	0.23	0.23	0.23	0.20	0.22	0.20	0.21	0.21	0.19	0.22	0.22	0.21	0.23	0.20	0.17	0.10

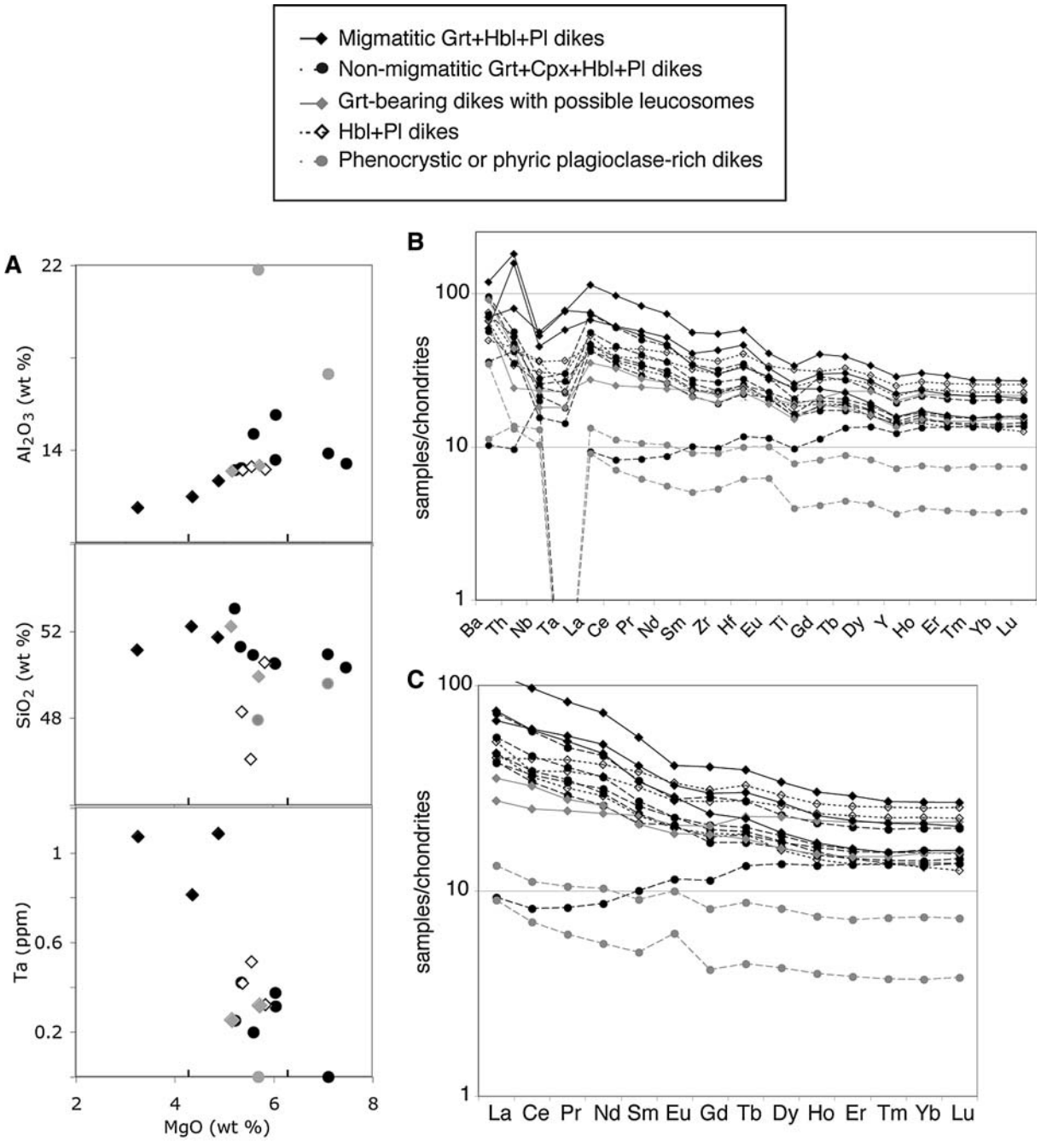

Fig. 5 Major and trace element compositions of Chipman mafic dikes. **a** Plots of Al_2O_3 (weight %), SiO_2 (weight %), and Ta (ppm) versus MgO (weight %). **b** Spider diagram for Chipman mafic dike samples. **c** REE diagram for Chipman mafic dike samples. Chrondrite values for both spider and REE diagrams from Sun and McDonough (1989)

SiO_2 and REE contents, suggesting it was least affected by crustal contamination.

Chipman mafic dikes and pegmatites

Whole rock Sm–Nd isotopic systematics were determined for the same 16 Chipman dike samples analyzed for major and trace elements. Fifteen of the Chipman dike samples reflect time-integrated LREE enrichment. One dike (02-112) has an isotopic composition characterized by time-integrated LREE depletion, consistent with the REE pattern indicated by whole rock geochemistry. The ε_{Nd} values at the time of 1.9 Ga granulite facies metamorphism range from −9.1 to +2.2 (Fig. 6c). A plot of ε_{Nd} values at 1.9 Ga versus weight percent SiO_2 for the 15 dikes characterized by time-integrated LREE enrichment reveals that dikes containing higher (>50.9%) SiO_2 content display an inverse correlation between ε_{Nd} and SiO_2, while three dikes with lower

Table 2 Sm-Nd isotopic data

Sample	[Sm][a]	[Nd][a]	$^{147}Sm/^{144}Nd$[b]	$^{143}Nd/^{144}Nd$[c]	ε_{Nd}	$\varepsilon_{Nd(initial)}$[d]	t_{CHUR}[e]	t_{DM}[f]
Chipman tonalite, 3.0 Ga								
SZ00-186C	4.24	29.31	0.08739	0.510297 ± 3	-45.66	-3.44	3.27	3.36
SZ00-193A	3.95	20.18	0.11833	0.510862 ± 4	-34.65	-4.40	3.47	3.56
SZ00-205A	9.02	54.11	0.10082	0.510641 ± 3	-38.96	-1.91	3.18	3.29
SZ00-208B	7.71	46.73	0.09973	0.510626 ± 8	-39.26	-1.79	3.17	3.28
Mafic granulite gneisses, 2.6 Ga								
Grt + Cpx + Opx + Pl granulites								
BF03-6B	2.95	11.89	0.14988	0.511770 ± 3	-16.94	-1.28	2.84	3.10
BF03-88A	2.54	7.94	0.19324	0.512592 ± 3	-0.90	0.69	2.03	3.75
BF03-159A	1.64	6.63	0.14912	0.511451 ± 4	-23.16	-7.29	3.82	3.91
BF03-168E	2.53	11.67	0.13096	0.511410 ± 3	-23.96	-1.98	2.86	3.05
BF03-228A	0.94	2.36	0.24094	0.513535 ± 4	17.5	2.72	3.10	2.70
Opx + Pl granulites								
BF03-92B	3.6	14.78	0.14724	0.511538 ± 3	-21.45	-4.94	3.40	3.55
BF03-125A	0.91	3.68	0.15009	0.511823 ± 4	-15.9	-0.31	2.67	2.97
BF03-158A	1.54	6.57	0.14202	0.511383 ± 5	-24.48	-6.23	3.51	3.63
BF03-189A	2.04	7.97	0.1545	0.511724 ± 3	-17.84	-3.74	3.31	3.51
BF03-217A	3.04	14.06	0.13093	0.511480 ± 4	-22.6	-0.6	2.69	2.91
Chipman mafic dikes, 1.9 Ga								
Migmatitic Grt + Hbl + Pl dikes								
02-125	5.65	21.02	0.1624	0.511840 ± 3	-15.56	-7.23	3.56	3.73
02-58	8.19	33.11	0.1495	0.511843 ± 3	-15.51	-4.02	2.58	2.89
99B-15	4.98	20.65	0.1459	0.511812 ± 3	-16.11	-3.75	2.49	2.80
Non-migmatitic Grt + Cpx + Hbl + Pl dikes								
02-112	1.45	3.79	0.2315	0.513183 ± 4	10.64	2.16	2.39	0.27
SZ00-182A	4.91	20.26	0.14644	0.511915 ± 4	-14.11	-1.86	2.20	2.58
SZ00-182B	3.76	15.89	0.1430	0.511863 ± 4	-15.13	-2.04	2.21	2.56
SZ00-196D	3.77	14.59	0.1561	0.512051 ± 3	-11.45	-1.55	2.21	2.65
02-171C	3.41	13.07	0.1580	0.511737 ± 3	-17.57	-8.17	3.56	3.72
SZ00-201A	2.95	10.81	0.1648	0.511776 ± 3	-16.82	-9.08	4.13	4.20
Grt-bearing dikes with possible leucosomes								
02-171B	3.02	11.19	0.1629	0.511881 ± 3	-14.77	-6.55	3.42	3.63
SZ00-186A	3.38	10.83	0.1889	0.512477 ±2	-3.15	-1.24	3.14	3.82
Non-migmatitic Hbl + Pl dikes								
01M123C	3.59	14.05	0.1544	0.512032 ± 3	-11.81	-1.50	2.19	2.62
02-120B	5.75	19.51	0.1782	0.512368 ± 3	-5.27	-0.76	2.23	2.98
02-123B	4.49	16.14	0.1681	0.512322 ± 2	-6.16	0.83	1.69	2.42
Phenocrystic or phyric plagioclase rich dikes								
SZ00-200A	1.38	4.72	0.1764	0.512349 ± 7	-5.64	-0.70	2.18	2.91
02-172	0.68	2.50	0.1637	0.512116 ± 5	-10.18	-2.14	2.42	2.87
Pegmatites, 1.9 Ga								
02-76B	2.11	21.8	0.05842	0.510226 ± 3	-47.05	-13.39	2.67	2.78
02-77B	1.03	5.56	0.11185	0.510210 ± 4	-27.85	-7.19	2.57	2.77
03-126	0.09	0.38	0.14129	0.511795 ± 33	-16.45	-2.95	2.33	2.65

[a]Concentrations in ppm, as determined by isotope dilution
[b]Sm and Nd were fractionation corrected with an exponental law, normalizing to $^{152}Sm/^{147}Sm = 1.783$ and $^{146}Nd/^{144}Nd = 0.7219$, respectively. Internal errors in measured $^{147}Sm/^{144}Nd$ are $< 0.1\%$ (2σ SD)
[c]Measured $^{143}Nd/^{144}Nd$ with internal error (2σ SE)
[d]Initial ε_{Nd} calculated at 1.9 Ga for Chipman dikes and pegmatites, at 3.0 Ga for Chipman tonalite, and at 2.6 Ga for mafic granulite gneisses
[e]t_{CHUR} (Ga) calculated with $(^{147}Sm/^{144}Nd)_{CHUR} = 0.1967$ and $(^{143}Nd/^{144}Nd) = 0.512638$
[f]t_{DM} (Ga) $= (1/\lambda_{147})*\ln[((^{143}Nd/^{144}Nd)_{sample} - (^{143}Nd/^{144}Nd)_{DM})/((^{147}Sm/^{144}Nd)_{sample} - (^{147}Sm/^{144}Nd)_{DM})) + 1]$;
present day $(^{143}Nd/^{144}Nd)_{DM} = 0.513151$, $(^{147}Sm/^{144}Nd)_{DM} = 0.2137$

($< 50.9\%$) SiO_2 content lack this correlation (Fig. 6d). This observation suggests the influence of crustal assimilation on the subset of dikes, including the migmatitic dikes, containing higher SiO_2.

Sm–Nd data were acquired for three pegmatite samples that cross-cut Chipman mafic dikes. The pegmatites reflect variable involvement of older crust, with T_{DM} from 2.67 to 2.33 Ga. Nd signatures for two of three pegmatite samples are characterized by ε_{Nd} values at 1.9 Ga from −7.2 to −3.0 (Fig. 6a). Data for the third sample indicate a more evolved Nd isotopic signature, with an ε_{Nd} value at 1.9 Ga of −13.4.

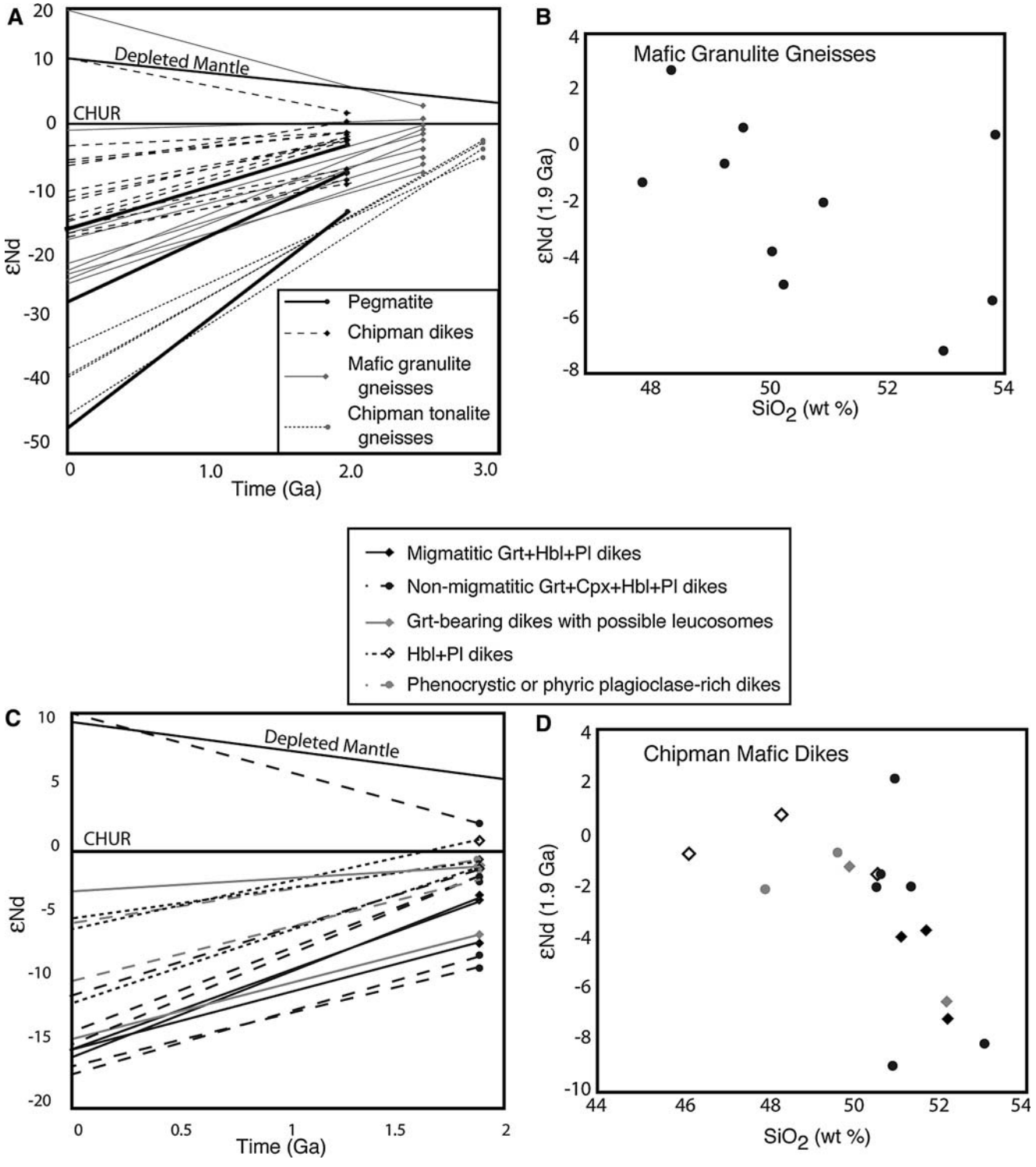

Fig. 6 **a** Nd isotope evolution diagram for Chipman mafic dikes corrected to 1.9 Ga, for pegmatite dikes corrected to 1.9 Ga, for mafic granulite gneisses corrected to 2.6 Ga, and for Chipman tonalitic gneisses corrected to 3.0 Ga. **b** Plot of ε_{Nd} at 2.6 Ga versus SiO_2 for mafic granulite gneisses. **c** Nd isotope evolution diagram for Chipman mafic dike samples corrected to 1.9 Ga. **d** Plot of ε_{Nd} at 1.9 Ga versus SiO_2 for Chipman mafic dikes. The inverse correlation between ε_{Nd} and SiO_2 for dikes with higher ($> 50.9\%$) SiO_2 content suggests the influence of crustal assimilation on this subset of dikes

U–Pb geochronology

Analytical methods

Mineral separation was accomplished using standard crushing, wilfley table, heavy liquid, and magnetic separation techniques. Representative zircon grains from selected samples were mounted in epoxy, polished to expose grain interiors, and characterized with cathodoluminescence (CL) and/or backscattered-electron (BE) imaging to document internal zoning (Figs. 7, 8). Zircon grains for analysis were either selected from this suite of imaged grains and extracted from the grain-mount, or hand-picked from the general population using the images as a guide. Single grain zircon fractions were photographed, air-abraded with pyrite after the method of Krogh (1982), measured, and rinsed and ultrasonicated in 3 M HNO_3. Zircon fractions dissolved early in the study were loaded with distilled acetone into Teflon FEP microcapsules, ultrasonicated and fluxed at ~80°C in 3 M HNO_3, and rinsed with several capsule volumes of 3 M HNO_3. Zircon fractions dissolved later in the study were loaded into savillex beakers, ultrasonicated and fluxed at ~80°C in 3 M HNO_3, rinsed in distilled acetone and high-purity water, and loaded into Teflon FEP microcapsules in high-purity water with no subsequent rinsing in the capsules. Samples were spiked with a mixed ^{205}Pb–^{233}U–^{235}U tracer, dissolved in 29 M HF at 220°C for 48–96 h, and converted to 6 M HCl at 180°C for 12–24 h. Pb and U were chemically separated using HCl anion exchange chemistry modified after Krogh (1973). Pb and U were loaded on single Re filaments with a silica gel 0.1 M H_3PO_4 emitter solution and analyzed

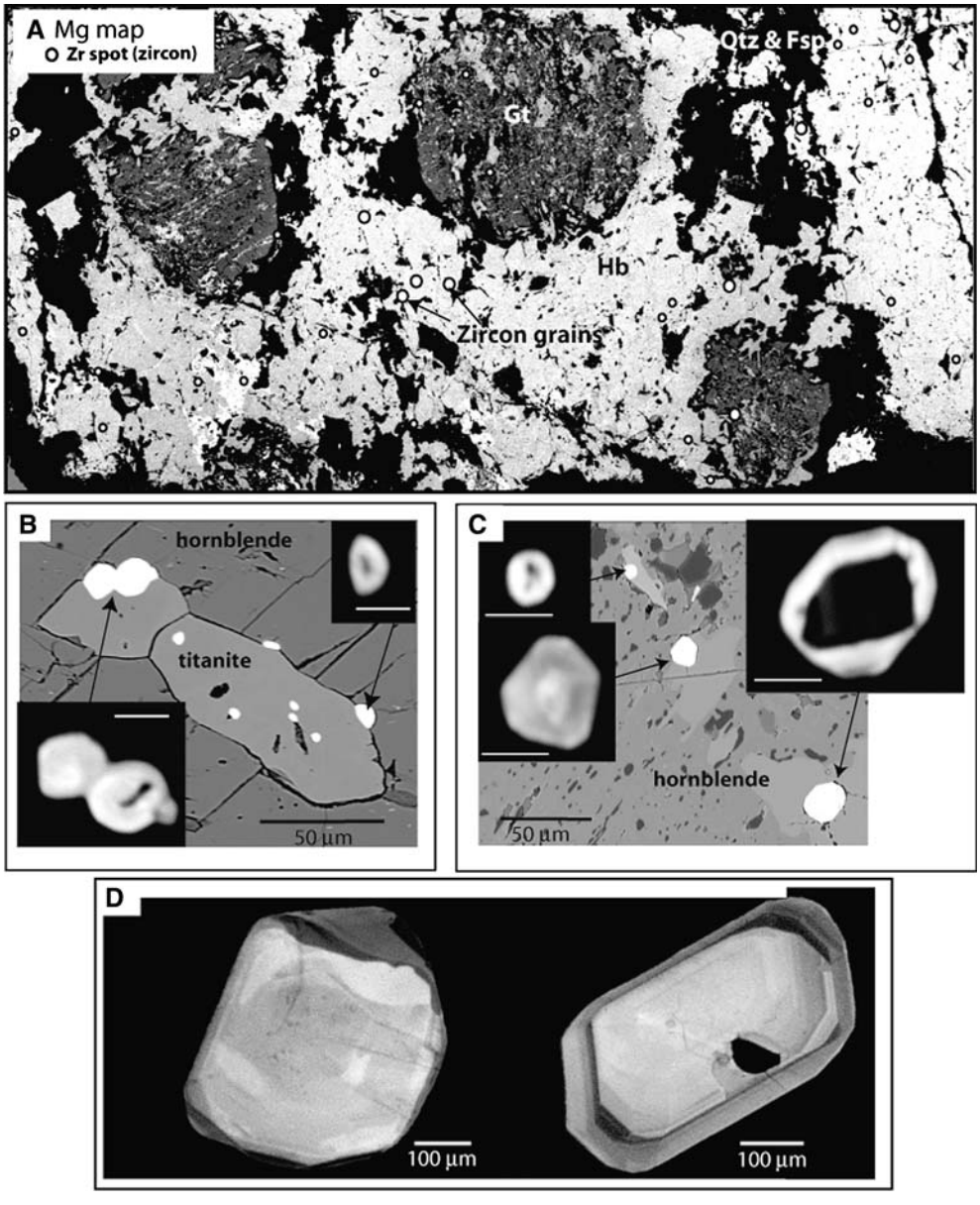

Fig. 7 **a** Mg map of thin section from SZ00-196C. Mineral phases are labeled. *White circles* mark locations of zircon grains. **b** Backscatter image showing petrographic setting of zircon crystals associated with titanite and hornblende. Insets are CL images of zircon grains with scale bars of 20 µm. **c** Backscatter image showing petrographic setting of zircon grains included in hornblende. Insets are CL images of zircon grains with scale bars of 10 µm. **d** CL images of larger zircon crystals that were physically separated from this sample

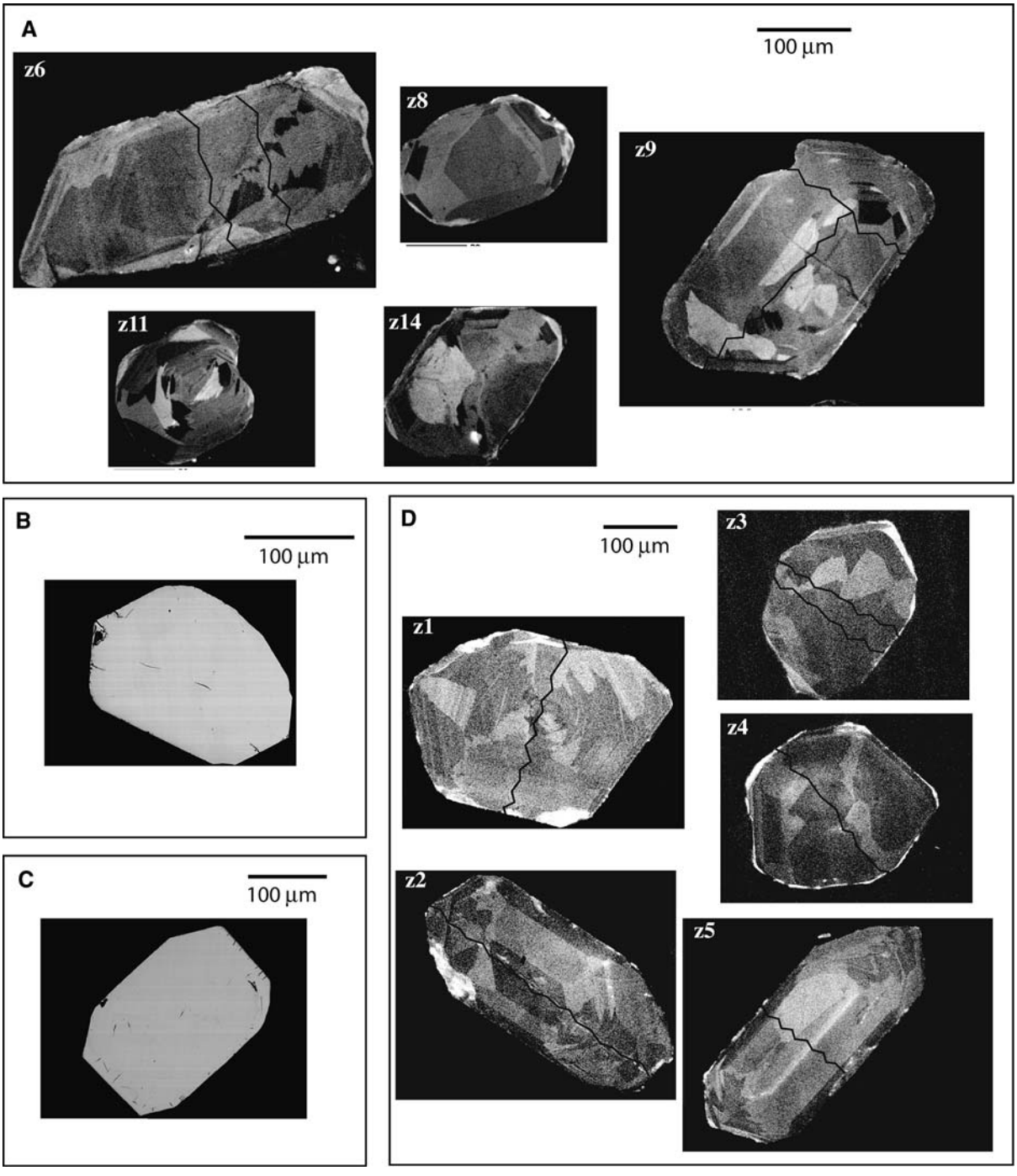

Fig. 8 **a** CL images of 03-52 zircon grains that were subsequently analyzed. Lines delineate where the zircon crystals were broken into fragments prior to analysis. **b**, **c** BE images of example 01-SZ76 and SZ00-196A zircon grains, respectively. **d** CL images of 02-76B zircon grains that were subsequently analyzed. Again, lines delineate where the crystals were broken into fragments

on the MIT VG Sector 54 mass spectrometer. Pb isotopic ratios were measured either by peak jumping using an axial counting Daly detector, or dynamically with Faraday cups and the Daly detector, peak-jumping ^{205}Pb into the axial position to obtain a real-time Faraday–Daly gain calibration. U was measured as an oxide, typically in static mode on three Faraday cups, and less commonly by peak-jumping into the Daly detector for smaller amounts of uranium. U–Pb data and details regarding isotopic ratio corrections are provided in Table 3. Concordia diagrams for all samples are shown in Figs. 9 and 10. Data are reported as ^{207}Pb/^{206}Pb weighted mean dates, except for samples with analyses characterized by higher discordance for which a York fit upper intercept date is reported. Decay constant and U–Pb tracer calibration uncertainties are systematic errors not included in the cited dates as they are unnecessary for comparison of dates within this dataset.

Sample selection

Five representative samples of migmatitic dikes were selected for U–Pb zircon analysis to place precise constraints on the timing of granulite facies metamorphism and anatexis (Fig. 3). Due to field observations suggesting episodic dike migmatization during sequential dike intrusion and metamorphism, rather than a single discrete period of anatexis postdating emplacement of the swarm, samples across the corridor of migmatitic dikes were targeted to test for spatial variability in the timing of dike migmatization. Morphological and internal zoning characteristics of zircon grains extracted from these samples, described further below, are consistent with metamorphic growth or crystallization in leucosomal melts (e.g., Corfu et al. 2003; Vavra et al. 1999). Although non-migmatitic dikes were also processed for accessory minerals, no zircon grains were recovered. This supports the interpretation of zircon growth owing to reactions associated with mafic dike anatexis, rather than due to igneous crystallization during dike intrusion.

Late, biotite-bearing, cross-cutting and variably deformed pegmatitic segregations and dikes intrude Chipman mafic dikes and other rocks of the Chipman domain. Four pegmatitic veins and dikes were selected for U–Pb zircon analysis to place a lower bound on felsic magmatism and local deformational fabrics in the Chipman domain.

Analytical results

Migmatitic dikes

Sample SZ00-196C, containing centimeter-scale garnet with centimeter-scale leucosome tails, was collected from a zone of exceptionally abundant migmatitic dikes at Woolhether Lake (Fig. 3). The distribution and petrographic setting of zircon grains in this sample was characterized by collection of major element and Zr thin section maps with the electron microprobe (Fig. 7a). Dozens of ovate to spherical zircon grains, typically <15 μm up to 40 μm in diameter, occur as inclusions in amphibole in one of several settings: in amphibole grains in the matrix, in amphibole inclusions in garnet, or associated with other inclusion phases in amphibole such as titanite (Fig. 7b, c). CL images commonly show distinct internal and external zircon domains of contrasting luminescence. Rare, irregular <30 μm zircon agglomerations were identified adjacent to garnet. Crushing procedures extracted clear to light pink zircon crystals that were large (up to 500 μm) prismatic and tabular, or small (<100 μm) spherical to ovate (Fig. 7d). Analyzed zircon grains were low U, with the lowest mean U concentrations in this study (<35 ppm), and low Th/U ratios (0.01–0.03). Six single grain and one multi-grain zircon fractions yielded a weighted mean $^{207}Pb/^{206}Pb$ date of 1896.7 ± 0.8 Ma (MSWD = 0.47) (Fig. 9a).

Sample 02-58 is a ~3 m wide dike from Chipman Lake that is migmatitic throughout its entire width and contains millimeter–centimeter scale leucosome stringers with small millimeter-scale garnet. Zircon grains are clear, spherical to ovate, typically <100 μm in diameter, with low Th/U ratios (0.05–0.10). Six single zircon grains yielded a weighted mean $^{207}Pb/^{206}Pb$ date of 1896.0 ± 0.7 Ma (MSWD = 1.83), excluding a seventh slightly older analysis (Fig. 9b).

Migmatitic dike sample 02-88, collected from Steinhauer Lake, contains coarse centimeter-scale garnet and asymmetric leucosome tails. Leucosomes in this dike contain both the earlier shallow northwest and the dominant northeast fabrics. Zircon grains are typically 60–120 μm in diameter, are clear and ovate to spherical in morphology, and are characterized by low Th/U ratios (0.01–0.08). Seven single grain zircon fractions yielded a weighted mean $^{207}Pb/^{206}Pb$ date of 1895.5 ± 0.5 Ma (MSWD = 0.39), excluding an eighth younger analysis (Fig. 9c).

Migmatitic dike sample 02-97 intrudes the Fehr granite east of Steinhauer Lake. This sample contained a discrete leucocratic segregation connected to veins emanating from centimeter-scale garnet and associated leucosome tails in the bulk of the dike (similar relationships shown in Fig. 4b). Zircon grains ranged from larger-sized (>150 μm) pink, prismatic, tabular to ovate crystals to smaller-sized (<150 μm) clearer, facetted, ovate to spherical crystals. Grains are characterized by low U concentrations (<42 ppm) and low Th/U ratios (0.01–0.02). Four single grain zircon fractions yielded a weighted mean $^{207}Pb/^{206}Pb$ date of 1896.8 ± 0.5 (MSWD = 0.81) (Fig. 9d).

Sample 03-52 is a somewhat atypical migmatitic dike, with remnant Grt + Cpx textures like that in the non-migmatitic garnet-bearing dikes. The dike is deformed, ranges in width from 30 to 150 cm, and intrudes Chipman tonalite on southern Chipman Lake. Zircon grains range from tabular and prismatic to facetted and spherical. Grain size ranges up to 400 μm in length for the tabular population, and is generally <150 μm for the spherical grains. CL images reveal internal irregular, sector-type zonation, outer shells of concentric zoning, and mineral inclusions such as apatite and quartz (Fig. 8a). Fourteen of sixteen zircon fractions were imaged prior to analysis. Zircon grains have low U concentrations (<85 ppm) and low Th/U ratios (0.02–0.08). Six zircon fractions yielded a weighted mean $^{207}Pb/^{206}Pb$ date of 1896.3 ± 0.5 Ma (MSWD = 0.45) (Fig. 9e), consistent with the data from the other migmatitic dikes. However, ten additional single zircon grains and fragments yielded a range of $^{207}Pb/^{206}Pb$ dates from 1898.9 ± 1.8 Ma to 2015.5 ± 1.1 Ma (Fig. 9f). We interpret the scatter of data along a discordant array trending toward a ca. 2.6 Ga upper intercept to indicate the presence of an inherited zircon component. A general correlation between Th/U ratio and zircon date is consistent with higher Th/U ratios in the inherited zircon portion.

Table 3 U-Pb ID-TIMS isotopic data for zircon

Fr	#[a]	Wt (μg)[b]	Compositions							Isotopic Ratios						Dates (Ma)					
			U (ppm)	Pb (ppm)	Th[c]/ U	Pb*[d]/ Pbc	Pbc[d] (pg)	$^{206}Pb^{e}/^{204}Pb$	$^{208}Pb^{f}/^{206}Pb$	$^{206}Pb^{f}/^{238}U$	% err[g]	$^{207}Pb^{f}/^{235}U$	% err[g]	$^{207}Pb^{f}/^{206}Pb$	% err[g]	$^{206}Pb^{h}/^{238}U$	$^{207}Pb^{h}/^{235}U$	$^{207}Pb^{h}/^{206}Pb$	±	corr. coef.	% disc.
SZ00-196C migmatitic dike																					
z1	1	18.7	11.2	3.7	0.02	26.3	2.6	1773.4	0.005	0.341950	(.13)	5.4736	(.15)	0.11609	(.08)	1896.0	1896.5	**1896.9**	1.4	0.867	0.1
z7	1	5.5	25.4	8.4	0.01	11.3	4.1	761.4	0.004	0.340374	(.58)	5.4417	(.59)	0.11595	(.11)	1888.5	1891.4	**1894.7**	2.0	0.981	0.4
z8	1	1.9	10.4	3.6	0.03	8.1	7.9	520.1	0.008	0.335973	(.66)	5.3788	(.67)	0.11611	(.09)	1867.3	1881.5	**1897.2**	1.7	0.990	1.8
z10	1	3.8	9.9	3.4	0.02	3.4	3.7	242.5	0.004	0.345060	(2.05)	5.5226	(2.08)	0.11608	(.25)	1911.0	1904.1	**1896.7**	4.5	0.993	-0.9
z11	2	5.5	19.6	6.8	0.03	6.7	5.3	444.9	0.009	0.342562	(.72)	5.4856	(.78)	0.11614	(.28)	1899.0	1898.3	**1897.6**	5.0	0.934	-0.1
z13	1	8.0	34.8	11.5	0.02	47.0	1.9	3157.5	0.005	0.341519	(.09)	5.4663	(.12)	0.11608	(.07)	1894.0	1895.3	**1896.8**	1.3	0.795	0.2
z14	1	2.0	17.7	5.8	0.02	13.3	0.9	904.3	0.004	0.342571	(.25)	5.4877	(.32)	0.11618	(.20)	1899.0	1898.7	**1898.3**	3.6	0.778	0.0
02-58, migmatitic dike																					
z2	1	0.8	96.1	32.4	0.10	53.8	0.5	3530.3	0.029	0.341698	(.10)	5.4662	(.13)	0.11602	(.08)	1894.8	1895.3	**1895.8**	1.4	0.809	0.1
z3	1	1.0	117.9	39.3	0.07	103.3	0.4	6826.2	0.019	0.341434	(.09)	5.4610	(.12)	0.11600	(.07)	1893.6	1894.5	**1895.5**	1.2	0.820	0.1
z6	1	2.3	208.7	69.7	0.06	73.3	2.1	4576.7	0.016	0.340854	(.09)	5.4518	(.13)	0.11600	(.08)	1890.8	1893.0	**1895.5**	1.5	0.743	0.3
z7	1	1.9	129.6	43.2	0.07	107.5	0.8	7095.0	0.021	0.341274	(.07)	5.4592	(.09)	0.11602	(.05)	1892.8	1894.2	**1895.8**	1.0	0.785	0.2
z8	1	1.1	188.2	62.7	0.06	60.8	1.1	3980.1	0.018	0.341268	(.12)	5.4591	(.13)	0.11602	(.05)	1892.8	1894.2	**1895.7**	0.9	0.918	0.2
z9	1	1.1	123.7	41.6	0.09	43.4	1.1	2843.4	0.027	0.342011	(.19)	5.4713	(.20)	0.11602	(.06)	1896.3	1896.1	**1895.8**	1.1	0.956	0.0
z10	1	1.1	203.3	67.6	0.05	75.3	1.0	4999.3	0.016	0.341736	(.06)	5.4720	(.08)	0.11613	(.05)	1895.0	1896.2	**1897.5**	1.0	0.765	0.2
02-88, migmatitic dike																					
z1	1	6.4	52.5	17.8	0.02	24.4	4.5	1509.1	0.005	0.340300	(.15)	5.4474	(.23)	0.11610	(.17)	1888.1	1892.4	**1897.0**	3.1	0.668	0.5
z4	1	7.0	61.2	20.1	0.02	44.4	3.2	2984.0	0.005	0.340722	(.09)	5.4472	(.11)	0.11595	(.06)	1890.1	1892.3	**1894.7**	1.1	0.814	0.3
z6	1	3.4	57.7	19.6	0.01	11.7	5.5	769.3	0.004	0.341555	(.40)	5.4658	(.41)	0.11606	(.10)	1894.1	1895.2	**1896.4**	1.8	0.971	0.1
z10	1	1.0	190.9	65.4	0.02	10.8	6.1	704.3	0.005	0.341870	(.41)	5.4702	(.43)	0.11605	(.11)	1895.7	1895.9	**1896.2**	1.9	0.969	0.0
z11	1	0.4	320.6	106.1	0.05	22.2	2.0	1489.4	0.013	0.340360	(.21)	5.4467	(.23)	0.11606	(.10)	1888.4	1892.2	**1896.4**	1.8	0.909	0.5
z12	1	3.9	36.8	13.1	0.05	6.7	7.1	438.6	0.014	0.341306	(.56)	5.4603	(.70)	0.11603	(.39)	1893.0	1894.4	**1895.9**	6.9	0.837	0.2
z13	1	3.8	51.3	17.0	0.02	15.0	4.3	1001.0	0.005	0.339851	(.41)	5.4344	(.42)	0.11597	(.07)	1886.0	1890.3	**1895.1**	1.3	0.984	0.6
z15	1	1.3	85.7	28.6	0.08	39.0	1.0	2578.7	0.024	0.340492	(.10)	5.4285	(.12)	0.11563	(.07)	1889.0	1889.4	**1889.7**	1.3	0.810	0.0
02-97, migmatitic dike																					
z1	1	22.0	34.9	11.6	0.01	73.8	3.4	4572.3	0.003	0.341661	(.06)	5.4708	(.08)	0.11613	(.04)	1898.0	1897.3	**1896.6**	0.8	0.804	0.2
z2	1	9.6	13.8	4.5	0.01	61.3	0.7	4116.7	0.004	0.341501	(.09)	5.4645	(.11)	0.11605	(.06)	1896.4	1896.3	**1896.2**	1.1	0.819	0.1
z3	1	6.0	42.1	14.0	0.01	38.4	2.2	2434.3	0.003	0.342030	(.10)	5.4727	(.12)	0.11605	(.06)	1894.7	1896.0	**1897.5**	1.2	0.847	0.0
z4	1	6.0	33.7	11.6	0.02	17.6	3.8	1097.8	0.004	0.342357	(.12)	5.4790	(.14)	0.11607	(.06)	1893.9	1895.0	**1896.3**	1.2	0.889	-0.1
03-52, migmatitic dike																					
z3	1	2.9	39.8	13.6	0.02	24.9	5.2	1533.2	0.007	0.342213	(.09)	5.4850	(.11)	0.11625	(.06)	1897.3	1898.2	**1899.3**	2.6	0.856	0.1
z4	1	9.8	42.8	14.9	0.06	20.2	3.5	1248.4	0.016	0.344244	(.18)	5.5571	(.20)	0.11708	(.09)	1907.1	1909.5	**1912.1**	1.0	0.891	0.3
z6a	1	5.0	36.6	12.2	0.05	95.1	1.1	6240.2	0.013	0.342117	(.19)	5.4740	(.20)	0.11605	(.06)	1896.8	1896.5	**1896.2**	1.7	0.956	0.0
z6b	1	8.8	62.8	21.7	0.04	17.9	4.7	1104.1	0.010	0.341996	(.12)	5.4731	(.18)	0.11607	(.14)	1896.3	1896.4	**1896.5**	1.1	0.662	0.0
z8	1	4.0	25.9	8.7	0.06	41.3	1.1	2712.8	0.019	0.342698	(.30)	5.5099	(.31)	0.11661	(.07)	1899.6	1902.1	**1904.9**	2.5	0.978	0.3
z9a	1	5.3	42.8	14.8	0.09	25.5	1.7	1609.5	0.025	0.345985	(.19)	5.6121	(.20)	0.11764	(.07)	1915.4	1918.0	**1920.7**	2.5	0.935	0.3
z9b	1	3.0	45.3	15.1	0.03	34.3	1.3	2242.5	0.007	0.341960	(.18)	5.4713	(.20)	0.11604	(.06)	1896.1	1896.1	**1896.1**	7.0	0.947	0.0
z11a	1	3.0	34.9	11.7	0.03	23.6	0.9	1583.6	0.009	0.345820	(.18)	5.6134	(.21)	0.11773	(.11)	1914.6	1918.2	**1922.0**	1.1	0.861	0.4
z11b	1	1.8	49.5	16.7	0.02	13.7	1.6	892.9	0.005	0.342122	(.39)	5.4747	(.41)	0.11606	(.12)	1896.9	1896.6	**1896.4**	2.4	0.955	0.0
z12a	1	1.3	51.7	17.0	0.02	77.0	0.7	5157.7	0.005	0.341983	(.09)	5.4723	(.11)	0.11606	(.06)	1896.2	1896.3	**1896.3**	2.2	0.847	0.0
z13a	1	3.0	47.3	17.2	0.36	34.7	1.9	2031.1	0.106	0.342147	(.15)	5.4943	(.17)	0.11647	(.07)	1897.0	1899.7	**1902.7**	1.0	0.902	0.3
z13b	1	3.8	49.7	17.1	0.03	13.0	2.0	837.1	0.008	0.342391	(.36)	5.4870	(.38)	0.11623	(.10)	1898.2	1898.6	**1899.0**	1.3	0.961	0.1

Table 3 (Contd.)

Fr	#[a]	Wt (μg)[b]	Compositions							Isotopic Ratios						Dates (Ma)					
			U (ppm)	Pb (ppm)	Th[c]/ U	Pb*[d]/ Pbc	Pbc[d] (pg)	$^{206}Pb^{e}/^{204}Pb$	$^{208}Pb^{f}/^{206}Pb$	$^{206}Pb^{f}/^{238}U$	% err[g]	$^{207}Pb^{f}/^{235}U$	% err[g]	$^{207}Pb^{f}/^{206}Pb$	% err[g]	$^{206}Pb^{h}/^{238}U$	$^{207}Pb^{h}/^{235}U$	$^{207}Pb^{h}/^{206}Pb$	±	corr. coef.	% disc.
z14	1	1.6	84.1	27.7	0.02	89.8	1.0	6006.7	0.007	0.341615	(.17)	5.4671	(.19)	0.11607	(.08)	1894.4	1895.4	**1896.5**	1.8	0.901	0.1
z15a	1	3.1	59.9	20.4	0.05	48.1	0.8	3193.2	0.014	0.348839	(.10)	5.7599	(.12)	0.11975	(.06)	1929.1	1940.4	**1952.5**	1.5	0.850	1.4
z15b	1	2.0	51.0	17.8	0.07	61.8	0.5	4061.4	0.020	0.355573	(.17)	6.0825	(.20)	0.12407	(.10)	1961.2	1987.7	**2015.5**	1.1	0.859	3.1
z16a	1	1.7	26.8	8.8	0.02	63.8	0.4	4272.7	0.006	0.341538	(.23)	5.4730	(.25)	0.11622	(.09)	1894.1	1896.4	**1898.9**	1.8	0.925	0.3
02-76B, pegmatitic dike																					
z1	1	22.0	48.6	17.3	0.34	265.8	1.4	15829.8	0.098	0.340802	(.12)	5.4457	(.14)	0.11589	(.07)	1890.5	1892.1	**1893.8**	1.2	0.873	0.2
z2a	1	1.8	61.9	22.4	0.40	37.1	1.1	2252.9	0.116	0.339989	(.23)	5.4157	(.25)	0.11553	(.10)	1886.6	1887.3	**1888.1**	1.7	0.927	0.1
z3a	1	6.0	249.6	86.6	0.25	512.1	1.0	32246.6	0.071	0.339825	(.06)	5.4197	(.07)	0.11567	(.04)	1885.8	1888.0	**1890.3**	0.8	0.787	0.3
z3b	1	8.3	207.8	72.1	0.24	523.2	1.1	32572.8	0.070	0.340224	(.05)	5.4272	(.07)	0.11569	(.04)	1887.7	1889.2	**1890.7**	0.7	0.794	0.2
z4a	1	4.5	154.2	54.1	0.28	230.1	1.1	14296.9	0.083	0.340207	(.07)	5.4252	(.09)	0.11566	(.05)	1887.7	1888.8	**1890.2**	0.9	0.831	0.2
z5a	1	7.0	60.9	21.7	0.32	86.3	1.8	5094.7	0.094	0.340516	(.07)	5.4331	(.09)	0.11572	(.06)	1889.2	1890.1	**1891.1**	1.0	0.782	0.1
02-77B, pegmatitic vein																					
z1	1	5.7	821.8	270.8	0.03	329.3	4.7	21293.7	0.009	0.340364	(.08)	5.4380	(.09)	0.11588	(.04)	1888.4	1890.9	**1893.6**	0.8	0.884	0.3
z7	1	8.0	1463.7	482.1	0.03	291.5	13.2	17885.1	0.008	0.340102	(.07)	5.4337	(.08)	0.11587	(.04)	1887.2	1890.2	**1893.5**	0.7	0.851	0.4
z12	1	0.7	401.6	132.5	0.04	124.2	0.7	8272.3	0.010	0.340890	(.05)	5.4455	(.08)	0.11586	(.06)	1890.9	1892.0	**1893.3**	1.0	0.700	0.1
z14	1	0.9	348.8	113.7	0.01	81.1	1.2	5447.3	0.003	0.338900	(.07)	5.4144	(.09)	0.11587	(.06)	1881.4	1887.1	**1893.5**	1.0	0.795	0.7
01-SZ26, pegmatitic segregation																					
z2	1	12.0	424.8	148.2	0.10	20.5	83.0	1218.7	0.028	0.338943	(.06)	5.4097	(.08)	0.11576	(.05)	1881.6	1886.4	**1891.7**	0.8	0.794	0.6
z3	1	1.3	465.2	154.9	0.08	81.3	2.4	5367.8	0.022	0.340323	(.19)	5.4299	(.20)	0.11572	(.07)	1888.2	1889.6	**1891.1**	1.2	0.941	0.2
z4	1	0.8	98.9	32.8	0.06	23.1	1.1	1546.2	0.018	0.339744	(.20)	5.4229	(.22)	0.11576	(.09)	1885.4	1888.5	**1891.8**	1.6	0.913	0.4
z7	1	3.4	681.4	225.3	0.07	146.5	5.2	9296.1	0.022	0.338478	(.07)	5.3978	(.08)	0.11566	(.04)	1879.3	1884.5	**1890.2**	0.8	0.852	0.7
z8	1	0.8	740.5	257.7	0.09	15.6	12.6	961.9	0.026	0.339045	(.14)	5.3978	(.15)	0.11547	(.05)	1882.1	1884.5	**1887.2**	1.0	0.932	0.3
z9	1	0.9	519.6	172.7	0.09	25.8	5.7	1636.7	0.026	0.339339	(.19)	5.4133	(.21)	0.11570	(.07)	1883.5	1887.0	**1890.8**	1.3	0.940	0.4
z10	1	1.0	767.1	254.9	0.08	114.6	2.2	7554.0	0.022	0.339554	(.14)	5.4175	(.15)	0.11571	(.07)	1884.5	1887.6	**1891.1**	1.2	0.905	0.4
SZ00-196A, pegmatite vein																					
z1	1	9.8	678.5	228.0	0.09	68.5	32.2	4084.1	0.025	0.338172	(.08)	5.3993	(.09)	0.11580	(.04)	1877.9	1884.7	**1892.3**	0.8	0.879	0.9
z2	1	27.3	721.2	241.3	0.09	172.0	24.1	10255.5	0.027	0.338902	(.09)	5.4138	(.10)	0.11586	(.04)	1881.4	1887.0	**1893.3**	0.7	0.913	0.7
z3	1	1.8	506.1	168.3	0.10	90.6	3.3	5944.7	0.028	0.338079	(.14)	5.4008	(.15)	0.11586	(.05)	1877.4	1885.0	**1893.3**	0.9	0.934	1.0
z4	1	1.3	1629.6	549.1	0.11	85.5	8.3	5238.1	0.031	0.339258	(.06)	5.4261	(.08)	0.11600	(.04)	1883.1	1889.0	**1895.5**	0.8	0.826	0.8
z7	1	2.0	606.4	198.4	0.07	139.4	2.8	9186.8	0.022	0.334489	(.09)	5.3409	(.11)	0.11581	(.06)	1860.1	1875.4	**1892.5**	1.1	0.834	2.0
z8	1	6.8	1870.8	632.5	0.08	47.3	88.9	2804.8	0.024	0.338143	(.14)	5.3972	(.15)	0.11576	(.04)	1877.7	1884.4	**1891.8**	0.8	0.955	0.9

[a]Number of grains in fraction
[b]Sample weights were estimated to within 40% using measured grain dimensions and a nominal density of 4.5 g/cm^3 for zircon.
[c]Th contents calculated from radiogenic ^{208}Pb and the $^{207}Pb/^{206}Pb$ date of the sample, assuming concordance between U-Th-Pb systems.
[d]Pb* and Pbc represent radiogenic Pb and common Pb respectively.
[e] Measured ratio corrected for fractionation and spike contribution; Pb fractionation was 0.12 ±0.04%/a.m.u. for Faraday detector or 0.20 ± 0.04%/a.m.u. for Daly detector analysis, based on daily analysis of NBS-981.
[f]Measured ratios corrected for fractionation, spike, blank, and initial common Pb; nominal U blank = 0.1 pg ± 50% (2σ); nominal Pb blank = 3.5 pg ± 50% (2s) for all zircon analyses except samples 02-58, 02-97, 03-52, 02-76B for which a Pb blank of 1.0 ± 50% (2σ) is applied; initial Pb composition estimated using the model for terrestrial Pb evolution of Stacey and Kramers (1975) at the nominal age of the fraction (i.e. 1.9 Ga).
[g]Numbers in parentheses are the % errors reported at the 2 sigma confidence interval, propagated using the algorithms of Ludwig (1980).
[h]Isotopic ages calculated using the decay constants of Jaffey et al. (1971): $\lambda(^{235}U) = 9.8485\times10^{-10}$ yr^{-1} and $\lambda(^{238}U) = 1.55125\times10^{-10}$ yr^{-1} ; error in $^{207}Pb/^{206}Pb$ date reported at the 2 sigma confidence interval.

Analyses of fragments from single zircon grains yield dates of 1,896 Ma, as well as older dates (e.g., z9a and z9b dates of 1920.7 ± 2.5 and 1896.1 ± 7.0 Ma, respectively, and z11a and z11b dates of 1922.0 ± 1.1 and 1896.4 ± 2.4 Ma, respectively), and are similarly consistent with inheritance.

Pegmatitic dikes and segregations

Sample 02-76B is a 40–50 cm wide biotite-bearing pegmatite dike that cross-cuts a deformed non-migmatitic garnet-bearing dike at Chipman Lake. Zircon grains are up to 500 μm in length, brown, prismatic, and either tabular or ovoid in morphology. U concentrations and Th/U ratios in analyzed zircon grains range from 15 to 85 ppm, and 0.24 to 0.40, respectively. CL images show irregular zoning in both tabular and ovoid zircon crystals (Fig. 8d), with occasional xenocrystic cores. Six single zircon fragments yielded a weighted mean $^{207}Pb/^{206}Pb$ date of ca. 1,891 Ma (Fig. 10a).

Sample 02-77B is an irregular 10–25 cm wide biotite-bearing pegmatitic vein that intrudes a migmatitic dike at Steinhauer Lake. Zircon grains are typically 150–250 μm in length (up to 400 μm), pinkish-brown, prismatic, and tabular, with common inclusions, and are characterized by Th/U ratios of 0.01–0.04. High U contents (350–1,500 ppm), radiation damage, and inferred low temperature Pb loss in this sample, as in the two previous pegmatite samples, contributed to significant discordance in most analyzed grains, such that only the four most concordant analyses of fifteen analyzed grains are reported in Table 3. Targeting of smaller-sized grains for analysis improved zircon concordance. The upper intercept date of a York fit through these four zircon analyses is 1893.4 ± 0.9 Ma (MSWD = 0.94) (Fig. 10b).

Sample 01-SZ26 is an irregular pegmatite vein from Woolhether Lake that intrudes Chipman tonalite adjacent to a migmatitic dike. Zircon grains from this sample are large (up to 300 μm), pinkish brown, and high in U (up to 770 ppm), with Th/U ratios from 0.06 to 0.1. The grains have good crystal faces, are tabular to ovate, and do not luminesce in CL. BE images are relatively homogeneous, (Fig. 8b) but reveal extensive fracturing in most grains, common alteration along fractures, and the presence of occasional xenocrystic cores. Six single zircon grains have $^{207}Pb/^{206}Pb$ dates from 1890.2 ± 0.8 to 1891.7 ± 0.8, with an additional analysis distinguishably younger at 1887.2 ± 1.0 Ma (Fig. 10c). Up to 0.7% discordance, as well as high common Pb in several analyses, is attributed to the somewhat metamict, fractured nature of the grains due to high U content. Excluding the two youngest analyses, five zircon fractions yielded a York fit upper intercept date of 1890.8 ± 1.4 Ma (MSWD = 0.55).

Sample SZ00-196A is a biotite-bearing pegmatite dike that intrudes a zone of extensive migmatitic dikes at Woolhether Lake. The sample was collected from the same outcrop as migmatitic dike sample SZ00-196C. Internally, the pegmatite dike lacks a fabric, but is broadly folded at the outcrop scale. Zircon grains are typically hundreds of microns in diameter, pinkish-

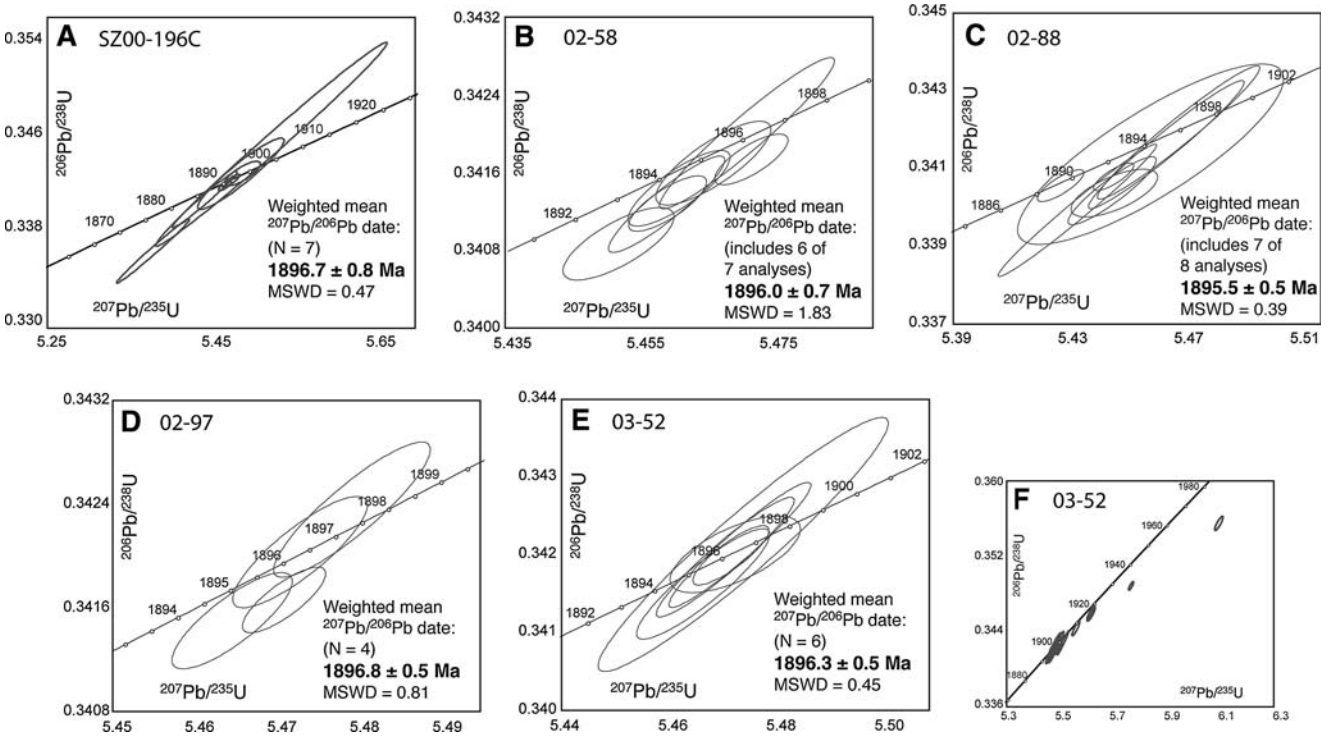

Fig. 9 Concordia diagrams for migmatitic dikes

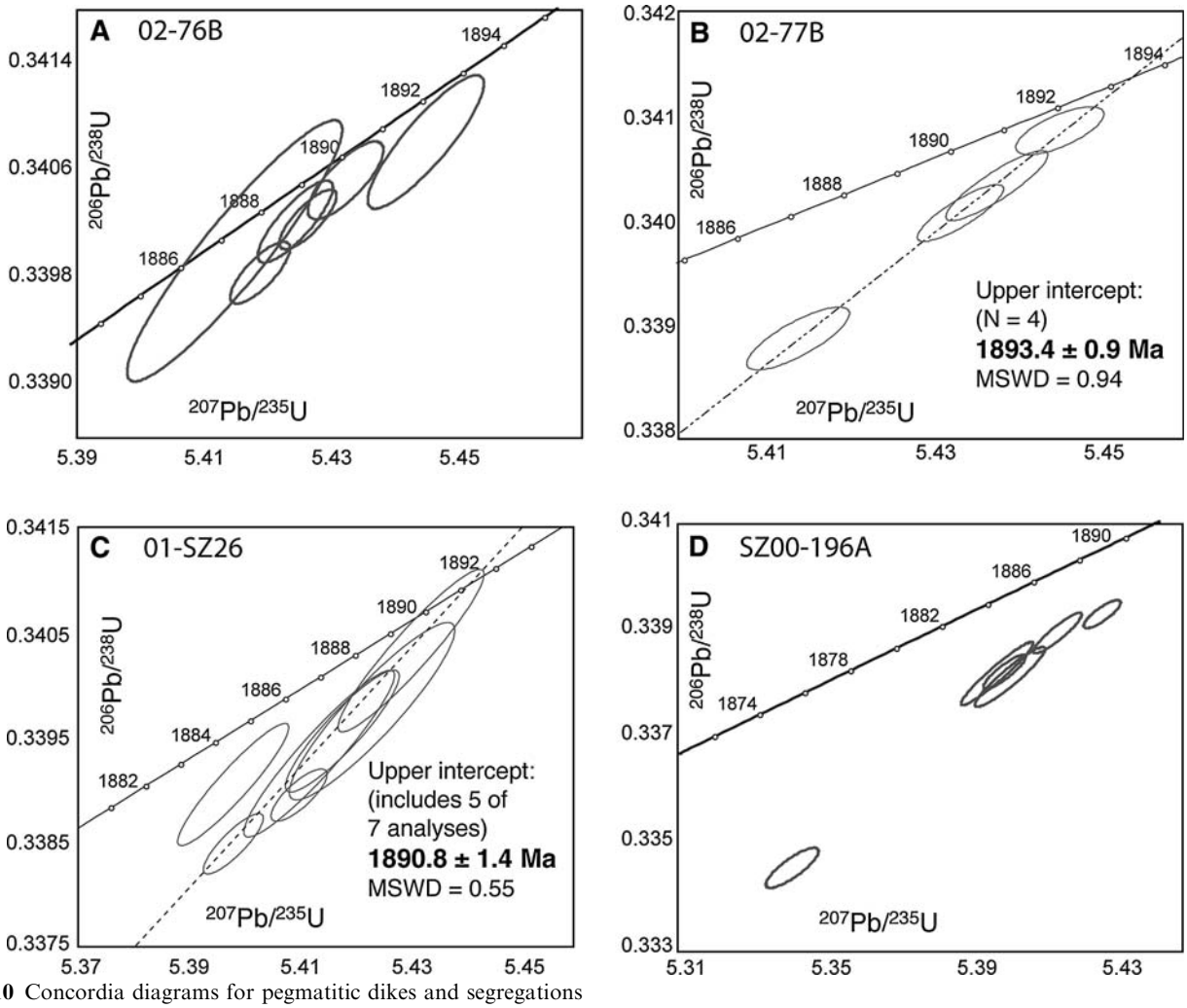

Fig. 10 Concordia diagrams for pegmatitic dikes and segregations

brown, prismatic, tabular to ovoid, and do not luminesce in CL. BE images generally show little internal structure, except for rare cores, and some alteration along fractures (Fig. 8c). Zircon grains contain the highest mean U contents of the study (500–1,900 ppm) and Th/U ratios of 0.07–0.11. High U concentrations, radiation damage, and associated low temperature Pb loss are likely responsible for the 0.7–2.0% discordance of six fractions reported in Table 3, and the significantly greater discordance in other fractions analyzed from this sample. $^{207}Pb/^{206}Pb$ dates range from 1891.8 ± 0.8 to 1895.5 ± 0.8 Ma (Fig. 10d).

Discussion

Sources of 1.9 Ga magmatism

Derivation of Chipman mafic dikes and pegmatites

Sm–Nd isotopic data impose some constraints on the sources of Proterozoic magmatism in the Chipman domain. Chipman mafic dike ε_{Nd} values at 1.9 Ga range from −9.1 to +2.2. Dikes with higher (> 50.9%) SiO_2 content display an inverse correlation between ε_{Nd} and SiO_2, suggesting the influence of crustal assimilation on these dikes (Fig. 6d). Contamination of the Chipman dikes by a component such as the host Chipman tonalitic gneisses, characterized by evolved Nd isotopic signatures (present-day ε_{Nd} values from −45.7 to −35.0), can explain the Chipman dike Nd and geochemical pattern.

The Nd isotopic signatures of two pegmatite samples are characterized by ε_{Nd} values at 1.9 Ga from −7.2 to −3.0. Comparison with the Nd isotopic signatures of the Chipman tonalite, mafic granulite gneisses, and Chipman mafic dikes indicates that the pegmatite data are consistent with derivation by melting of either the mafic gneisses (ε_{Nd} values at 1.9 Ga from −11.6 to −0.1) or Chipman mafic dikes (ε_{Nd} values at 1.9 Ga from −9.1 to +2.2) (Fig. 6a). These pegmatite data are incompatible with generation by melting of Chipman tonalitic gneisses, as Chipman tonalite ε_{Nd} values at 1.9 Ga were too evolved, ranging from −19.1 to −16.0. The ε_{Nd} value at 1.9 Ga for a third pegmatite sample is −13.4. It is consistent with genesis from the same source as the other

analyzed pegmatites, but the more evolved Nd isotopic signature suggests a greater contribution from a component like the Chipman tonalite.

Comparison with sources of other Proterozoic magmas in the western Churchill Province

The Chipman mafic dike whole rock geochemical and Nd isotopic data also allow comparison with the inferred sources for other Proterozoic magmas across the western Churchill Province. The Chipman mafic dike HFSE depletions and LILE enrichments are characteristic of arc magmas, and could reflect (1) derivation from enriched lithospheric mantle previously affected by subduction-related processes as has been interpreted elsewhere in the western Churchill Province, or (2) derivation from depleted lithospheric mantle or asthenosphere and assimilation of subduction related felsic intrusives. The ca. 1.83 Ga ultrapotassic rocks of the Christopher Island Formation, intruded across a large area in the northern part of the western Churchill Province, contain arc-like trace element patterns, are characterized by ε_{Nd} values at 1,830 Ma from −10.5 to −6, and lack a clear correlation of ε_{Nd} value with SiO_2 content. These data have been interpreted to represent derivation of the Christopher Island Formation from an extensive enriched reservoir isolated since an Archean metasomatic subduction-related event, with limited crustal contamination during emplacement (Cousens et al. 2001). The ca. 2.45 Ga Kaminak dikes, ca. 2.19 Ga Tulemalu dikes, and ca. 2.2 Ga basaltic flows of the western Churchill Province have similarly been inferred to contain a contribution from an enriched component (Cousens et al. 2001; Sandeman et al. 2003). As discussed above, the correlation of Chipman mafic dike ε_{Nd} value with SiO_2 content implies the influence of crustal assimilation on dike geochemistry. Exclusion of dikes with higher SiO_2 content yields more restricted 1.9 Ga ε_{Nd} values from −2.1 to 2.2. These latter values do not overlap with the Christopher Island Formation envelope of ε_{Nd} values. Because the primary Nd isotopic signature of the Chipman mafic dikes has been obscured by crustal assimilation, contribution from a minor enriched lithospheric mantle component as inferred for other Proterozoic intrusives cannot be excluded. However, the Chipman mafic dike geochemical and isotopic signature suggests derivation from a predominantly depleted lithospheric or asthenospheric mantle source with assimilation of older subduction-related intrusives during emplacement.

Evolution of 1.9 Ga deep crustal thermal regime

Intensity of high-P granulite facies metamorphism

Chipman dike metamorphic assemblages, thermobarometric data, and the extent of melting in host felsic gneisses allow us to evaluate the intensity of Chipman dike high-P metamorphism. Migmatitic and non-migmatitic dikes record conditions of 750–850°C, 1.0–1.2 GPa (Williams et al. 1995), and are considered minimum temperature estimates because of evidence for diffusional reequilbration. This is compatible with a variety of experimental studies demonstrating that vapor-absent melting of mafic rocks at 1.0–1.2 GPa can occur at temperatures of 850–1,000°C (e.g., Rapp et al. 1991; Rushmer 1991; Patino Douce and Beard 1995; Rapp and Watson 1995; Springer and Seck 1997), and possibly as low as 750°C (Wolf and Wyllie 1993, 1994, 1995).

Despite similar *P–T* constraints for dikes across the swarm, only a subset underwent anatexis. Our field and geochemical data suggest that composition may be an important factor. Internal dike-parallel banding of migmatitic and non-migmatitic textures within a single dike is consistent with successive intrusion of compositionally varying magma batches that may have controlled dike reaction history. Geochemical data suggest that typical migmatitic dikes are characterized by higher SiO_2, Fe_2O_3, HFSEs and REEs, and lower MgO and Al_2O_3 than typical non-migmatitic dikes. These compositional variations cannot be simply explained by inappropriate integration of melanosomal and leucosomal fractions during sampling of migmatitic dikes (for example, SiO_2 and Al_2O_3 are not positively correlated). The inverse correlation between ε_{Nd} and SiO_2 for migmatitic dikes suggests that assimilation of older crustal material may have increased the SiO_2 content of some dike magma batches, and thus made these dikes more susceptible to subsequent migmatization. Williams et al. (1995) previously proposed that SiO_2 content played a role in controlling dike reaction history. Similarly, the abundance of quartz has been interpreted as the primary control on reaction progress in migmatitic mafic granulite gneisses of the Kapuskasing Structural Zone (Hartel and Pattison 1996). This latter investigation also noted that variation in Fe exerted a secondary influence on migmatization, consistent with the higher Fe_2O_3 content of analyzed Chipman migmatitic dikes in our study.

Limited anatexis of host felsic gneisses during high temperature metamorphism suggests that the rocks were probably vapor absent prior to dike metamorphism. This represents an endmember response of the crust to granulite facies conditions. At pressures of 1.0–1.5 GPa, water-saturated tonalite melting occurs at relatively low temperatures of 625–650°C (e.g., Lambert and Wyllie 1974; Schmidt 1993), but the vapor absent tonalite solidus is defined by biotite and/or hornblende dehydration melting at minimum temperatures of 855–900°C (Skjerlie and Johnston 1993, 1996; Patino-Douce 2005). Compositional effects such as low Ca in the bulk tonalite or high Ti and F in biotite can extend the stability of hornblende and biotite to even higher temperatures (Skjerlie and Johnston 1993, 1996). At 1.0–1.5 GPa pressures, biotite dehydration occurs at lower tempera-

tures than amphibole dehydration, consistent with the observation of more abundant melts in the biotite-bearing Fehr granite than in the hornblende-bearing Chipman tonalite. We attribute the absence of free water in the felsic host gneisses to Archean metamorphism that left the Chipman domain rocks resistant to melting during subsequent Proterozoic metamorphism (Flowers 2005; Mahan et al. 2006).

We suggest that the entire Chipman domain was temporarily elevated to temperatures ≥750°C during Chipman dike intrusion and metamorphism. Spatial heterogeneity in patterns of mafic dike and tonalitic gneiss anatexis can be attributed to lateral peak temperature, geochemical and fluid activity variability. The attainment of the hottest temperatures that exceeded the dry amphibolite and tonalite solidi may in part be locally linked to successive intrusion and crystallization of dike magmas (e.g., Petford and Gallagher 2001). The susceptibility of both mafic dikes and heterogeneous felsic gneisses to anatexis, as discussed above, is also compositionally dependent. Fluid composition and activity may similarly play an important role in determining the dike reaction history. Thus, the complex interaction of thermal and compositional factors likely controlled melting of rocks in the Chipman domain during 1.9 Ga high-P granulite facies metamorphism.

Constraints on the timing and duration of metamorphism

Metamorphic zircon grains in Chipman migmatitic mafic dikes permit precise dating of anatexis during 1.9 Ga high-P granulite facies conditions. Field relationships, discussed previously, are most simply explained by synmetamorphic and syntectonic emplacement of the Chipman dikes, with episodic or continuous migmatization of dikes during intrusion (Williams et al. 1995). This suggests that dates for dike anatexis also constrain the timing of dike intrusion. The possibility that some dikes were emplaced at an earlier time cannot be entirely excluded, although broadly similar dike geochemistry patterns are consistent with mafic magma derivation from a single source region. Four migmatitic dikes distributed across the corridor of dike anatexis yield indistinguishable weighted mean $^{207}Pb/^{206}Pb$ dates from 1896.7 ± 0.8 to 1895.5 ± 0.5 Ma. A fifth migmatitic sample contains a population of 1896.3 ± 0.5 Ma zircon crystals, with additional grains characterized by minor inheritance. These data suggest that the time span for dike migmatization at exposed crustal levels was ≤ 2.5 m.y., established by the errors on the range of sample zircon dates. It is unclear whether the onset of high-grade conditions in the Chipman domain coincided with dike emplacement, or commenced at an earlier time. We consider the weighted mean 207Pb/206Pb date of 1896.2 ± 0.3 Ma for the thirty most concordant zircon grains from the five migmatitic mafic dike samples to be the best estimate for the timing of emplacement, high-P granulite facies metamorphism (> 750°C, 1.0–1.2 GPa), and anatexis of the Chipman dikes.

U–Pb titanite data support the continued elevation of temperatures ≥550–650°C (above the U–Pb closure temperature of titanite; e.g., Hanson et al. 1971; Cherniak 1993) following anatexis of currently exposed Chipman mafic dikes. Titanite grains from six samples distributed across the Chipman domain yielded dates from 1,898 to 1,882 Ma (Flowers et al. 2006). This implies either that temperatures ≥600–650°C were heterogeneously maintained for 14 m.y. following of Chipman dike anatexis, or that parts of the domain were reheated following immediate post-1,896 Ma cooling. These data suggest the ongoing persistence of a heat source following mafic dike intrusion and anatexis.

U–Pb zircon and Sm–Nd whole rock data for pegmatites similarly imply protracted maintenance of high temperatures at deeper crustal levels following anatexis of currently exposed dikes. Four cross-cutting pegmatitic veins and segregations yielded U–Pb dates from 1893.4 ± 0.9 to 1890.8 ± 1.4 Ma, distinctly postdate the timing of 1,896 Ma migmatization of exposed dikes, and impose a lower bound for major magmatism and deformation in Chipman domain exposures. As discussed previously, the Nd isotopic signatures of several pegmatite samples are consistent with derivation from either the mafic gneisses or Chipman mafic dikes. Pegmatite generation from melting of mafic lithologies by amphibolite anatexis requires temperature > 750°C, which we interpret to signify the continuation of granulite facies conditions at somewhat deeper crustal levels. Pegmatite emplacement in cross-cutting geometries from 1,894 to 1,891 Ma thus reflects intrusion into a cooler thermal regime at the shallower currently exposed levels, postdating earlier 1,896 Ma higher temperature anatexis of Chipman mafic dikes at this depth. High temperature cooling from 1,896 to 1,894–1,891 Ma at the current level of exposure may be due to a degree of unroofing associated with extension during mafic dike emplacement, or initial decay of the thermal event. However, as noted above, the titanite data constrain temperatures ≥600–650°C in portions of the domain through 1,882 Ma. Together, these constraints on the evolution of the thermal regime suggest a somewhat protracted (~14 m.y.) metamorphic event following attainment of peak conditions.

Implications for lithospheric reactivation and mantle dynamics

Correlation of mafic magmatism

The intrusion and metamorphism of the 1896 Ma Chipman mafic dike swarm is part of a major episode of Proterozoic mafic magmatism along the central Snowbird tectonic zone. In addition, the Virgin River dikes

are along-strike upper amphibolite facies mafic dikes exposed 400 km southwest of the Chipman dikes, are truncated on their eastern side by the Virgin River shear zone, and have previously been correlated with the Chipman dikes and LLSZ (Fig. 1) (Card 2002; Mahan et al. 2003). Further northeast in the Selwyn lozenge, 1.1 GPa, 800°C granulite facies mafic dikes intrude rocks similar to the Chipman tonalite and are similarly truncated on their eastern side by a thrust sense shear zone considered the continuation of the LLSZ (Mahan and Williams 2005). The NE striking Kazan dikes 400 km northeast of the East Athabasca region contain remnant garnet and clinopyroxene, have yielded bulk K–Ar dates of ca. 1.9 Ga, and intrude a 25–30 km wide zone along the Tulemalu fault zone (Fahrig et al. 1984) that has been correlated with the Virgin River and Legs Lake-Black Lake shear zones (Tella and Eade 1986). The similar relationships, kinematics, location and apparent timing of mafic dikes and shear zone for 800 km along strike provide strong evidence for a genetic link among these exposures. Thus, we suggest that the Chipman dikes can be correlated with mafic dikes for a minimum strike-length of 800 km along the Snowbird tectonic zone, establishing the Chipman dikes as a substantial mafic dike swarm of regional significance.

Intrusion of the extensive Chipman mafic dike swarm was approximately coincident with major mafic magmatism along the northern Snowbird tectonic zone, 600–800 km northeast of the East Lake Athabasca region. The 850 km^2 Kramanituar complex is dominated by granulite facies metagabbro, norite and anorthosite that was intruded at 1902 ± 1.6 Ma, with subsequent cooling through the 400–450°C closure temperature of rutile at ca. 1901 Ma (Sanborn-Barrie et al. 2001). Mafic granulite dikes in the Uvauk mafic complex are inferred to have a similar origin and age as mafic granulites in the Kramanituar complex (Mills et al. 2000). The 2,500 km^2 Daly Bay complex is an extensive body of mafic to anorthositic rocks, tonalite and paragneiss (Gordon 1988; Hanmer and Williams 2001) with preliminary 1.9 Ga zircon dates (M. Williams, personal communication). In addition, the subsurface extension of the Snowbird tectonic zone to the south has been inferred to record the opening and closure of a marginal Proterozoic ocean basin (Ross et al. 1995, 2000) (Fig. 1). Ocean basin development is tectonically compatible with coeval along-strike mafic magmatism. Together, these data indicate widespread distribution of 1.9 Ga mafic magmatism for >1,200 km of the Snowbird tectonic zone, and potential links to the south that would extend the correlation along the entire 2,800 km length of the geophysical lineament.

Asthenospheric upwelling and lithospheric reactivation

In the East Lake Athabasca region, evidence for a prolonged period of lithospheric stability preceding 1.9 Ga activity suggests that the Proterozoic event was severe enough to disrupt a stable Archean craton. Archean deep crustal granulite facies metamorphism at ca. 2.55 Ga has been interpreted in the Chipman, northwestern, and southern domains (Williams et al. 2000; Baldwin et al. 2004; Flowers 2005; Williams and Hanmer 2005; Mahan et al. 2006). With the exception of apparently minor lower crustal fluid flow events, there is essentially a hiatus in activity in these rocks until the second episode of high-P granulite facies metamorphism at 1.9 Ga. We interpret the recurrence of metamorphism at high-P, with an intervening quiescent interval, to imply an ~650 m.y. period of deep crustal residence and lithospheric stability prior to lithospheric disruption in the Proterozoic. This hypothesis is consistent with limited melting of the felsic gneisses during 1.9 Ga high-temperatures that implies these rocks were vapor-absent. We attribute this character to earlier dehydration during Archean granulite facies metamorphism that increased the resistance of these rocks to subsequent anatexis and deformation.

The widespread 1.9 Ga mafic magmatism along a feature spanning thousands of kilometers of the western Canadian Shield provides a robust basis for interpreting a continental-scale 1.9 Ga episode of asthenospheric upwelling that reflects significant mass and thermal input to the crust. The ca. 1.9 Ga activity along the Snowbird tectonic zone is spatially and temporally bounded by the 1.91–2.02 Ga Taltson-Thelon orogen to the northwest and the 1.81–1.91 Ga Trans-Hudson orogen to the southeast during final amalgamation of the western Canadian Shield. These two major, inward-dipping collision zones would have dramatically impacted the intervening Churchill Province lithosphere during the assembly of Laurentia. The northeast trending distribution of 1.9 Ga mafic magmatism along the Snowbird tectonic zone is consistent in orientation with these bounding orogens, and supports a link between these features.

We suggest that opening of an ocean basin along the southern Snowbird tectonic zone (Ross et al. 2000) may have been followed by propagation of an incipient continental rift along the central Snowbird tectonic zone (Fig. 11). Models to accommodate initial basin formation include (1) extension induced by a central zone of asthenospheric upwelling and lithospheric thinning as a convective response to the trench suction force exerted by lateral downgoing slab(s) (e.g., Bott 1982), and (2) hinterland transtension due to a strike-slip dominated regime initially driven by Slave collision in a manner analogous to Himalayan hinterland activity. The latter has been postulated for opening of a Proterozoic marginal basin, termed the Thorsby basin, along the southern Snowbird tectonic zone (Ross et al. 1995, 2000).

Although the boundary conditions may have been appropriate to induce only this local point of rupture, initiation would have facilitated its subsequent propagation in an overall tensional regime along a zone of asthenospheric upwelling. If the Snowbird tectonic zone

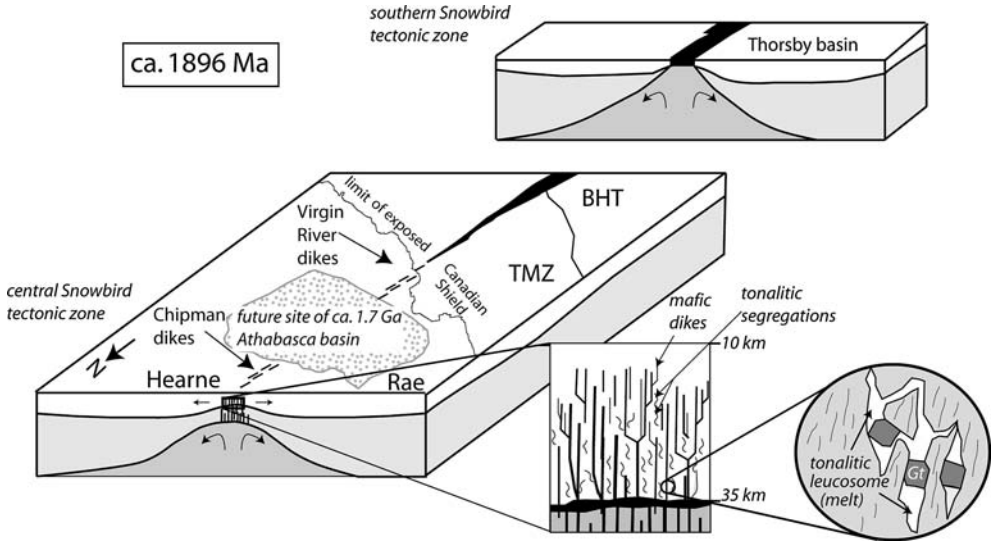

Fig. 11 Block diagram depicting the tectonic environment envisioned during 1,896 Ma Chipman mafic dike emplacement. View is to the south. Development of a Proterozoic marginal basin, the Thorsby basin, along the southern Snowbird tectonic zone (Ross et al. 2000), may have been followed by northward propagation of an incipient rift marked by intrusion of the Virgin River and Chipman mafic dikes. The traces of the dike swarms are shown at the surface in order to illustrate the distribution of the mafic magmatism, but in reality the dikes probably did not reach the surface. Insets show the emplacement of the Chipman mafic dikes in the deep crust and the generation of tonalitic melts through amphibolite anatexis. *BHT* Buffalo Head Terrane, *TMZ* Taltson Magmatic Zone

presented an ancestral NE-striking zone of lithospheric weakness, this may have further enhanced and guided Proterozoic rift propagation, as proposed for other continental rifts (e.g., Courtillot 1982). Ongoing study is being carried out to establish the significance and nature of Archean northeast-striking structures, and will clarify the control they may have exerted on subsequent tectonism. Regardless of the mechanism of propagation, mafic magmatism at 1,900–1,896 Ma along the central segment of the Snowbird tectonic zone is consistent with northward development of this nascent rift, with the Chipman mafic dike swarm representing the early stages of rift formation in the central Snowbird zone (Fig. 11). The enormous mafic complexes along the northern Snowbird tectonic zone (Kramanituar, Uvauk, Daly Bay) may represent separate, but related, development in extensional settings in response to the collision of the Slave and Rae provinces. The emplacement and exhumation of the 1.9 Ga Kramanituar complex has been attributed to extension in the Thelon hinterland driven by underthrusting of the Slave craton (Sanborn-Barrie et al. 2001).

Accretionary activity to the east associated with Trans-Hudson orogenesis may have induced a subsequent transition to hinterland contraction, contributing to basin closure along the southern Snowbird tectonic zone, terminating dike emplacement and incipient rifting along the central segment, and ending mafic complex development in the northern segment. Terminal collision of the Hearne and Superior cratons in the Trans-Hudson coincided with development of the 1,856–1,798 Ma Rimbey magmatic arc along the southern segment of the Snowbird tectonic zone, interpreted to reflect closure of the Proterozoic marginal ocean basin (Ross et al. 1995, 2000). This is temporally and kinematically consistent with ca. 1.85 Ga regional contractional uplift of the central segment of the Snowbird tectonic zone along the LLSZ (Mahan and Williams 2005; Mahan et al. 2006). The absence of a magmatic arc in the central Snowbird tectonic zone, along the zone of dike emplacement, may be due to the insufficient time necessary for an ocean basin to develop prior to the shift to regional contraction.

Propagation of an incipient continental rift at ca. 1.9 Ga along the Snowbird tectonic zone coherently links observations of mafic dike emplacement and speculated marginal ocean basin development along the central and southern segments, and is consistent with coincident mafic complex intrusion along the northern segment. Regardless of the mechanisms responsible for the intrusion of the 1.9 Ga mafic magmas, their distribution along thousands of kilometers of the Snowbird tectonic zone indicates a major episode of 1.9 Ga asthenospheric upwelling across the western Canadian Shield. The mafic magmatism along this lineament may also have been key in imparting the distinctive gravity and magnetic anomalies that define this fundamental geophysical feature. The assembly of the Laurentian supercontinent constituted a major period of ca. 1.9 Ga lithospheric reorganization in the western Chuchill Province. The extensive distribution of Proterozoic mafic magmas indicates that this event involved significant mass transfer from the mantle to the crust, and is an integral component of the unusual history of lithospheric reactivation and lower crustal exhumation preserved in the East Lake Athabasca region.

Conclusions

The Chipman domain of the East Lake Athabasca region in northern Saskatchewan preserves a spectacular record of 1.9 Ga deep crustal mafic magmatism, silicic melt generation and segregation, deformation, and high-P granulite facies metamorphism. Data indicate dike anatexis at 1,896.2 ± 0.3 Ma during conditions of 1.0–1.2 GPa, ≥750°C, intrusion of pegmatites from 1,894 to 1,891 Ma, and subsequent protracted maintenance of high temperatures that may be linked with ongoing mafic magma emplacement at somewhat greater depth. The Chipman dikes in the East Lake Athabasca region can be correlated with 1.9 Ga mafic magmatism spanning thousands of kilometers of the western Canadian Shield, indicating regional asthenospheric upwelling along the Snowbird tectonic zone. This record of deep crustal magmatism, metamorphism and exhumation follows an extended episode of quiescence, and is consistent with the destabilization of this portion of cratonic lithosphere during the assembly of Archean continental blocks in Laurentia.

Acknowledgements This research was supported by National Science Foundation grant EAR-0310215 to S.A. Bowring and M.L. Williams, and a NSF Graduate Fellowship and a GSA student research grant to R.M. Flowers. We thank Alexis Ault for two field seasons of exceptional and energetic assistance. Helpful discussions with Kevin Mahan, Greg Dumond, Rob Berman, Sally Pehrsson and Julie Baldwin are greatly appreciated. Thanks to Tim Grove for petrological insights and to Frank Dudas for geochemistry discussion and assistance with Sm–Nd data. We appreciate thoughtful reviews from Urs Schaltegger and Jim Mattinson that strengthened the manuscript.

References

Baldwin JA, Bowring SA, Williams ML (2003) Petrological and geochronological constraints on high pressure, high temperature metamorphism in the Snowbird tectonic zone. Can J Metamorph Geol 21:81–98

Baldwin JA, Bowring SA, Williams ML, Williams IS (2004) Eclogites of the Snowbird tectonic zone: petrological and U–Pb geochronological evidence for Paleoproterozoic high-pressure metamorphism in the western Canadian Shield. Contrib Mineral Petrol 147:528–548

Bott MHP (1982) The mechanism of continental splitting Tectonophysics 81:301–309

Card CA (2002) New investigations of basement to the western Athabasca Basin. In: Summary of Investigations v2, Saskatchewan Geological Survey, Sask Industry Resources, Miscellaneous Report, 2002–4.2 CD-ROM, Paper D-12, 17pp

Cherniak DJ (1993) Lead diffusion in titanite and preliminary results on the effects of radiation damage on Pb transport. Chem Geol 110:177–194

Corfu F, Hanchar JM, Hoskin PWO, Kinny P (2003) Atlas of zircon textures. In: Hancar JM, Hoskin PWO (eds) Zircon, reviews in mineralogy and geochemistry, vol 53. Washington, pp 468–500

Courtillot V (1982) Propagating rifts and continental breakup. Tectonics 1:239–250

Cousens BL, Aspler LB, Chiarenzelli JR, Donaldson JA, Sandeman H, Peterson TD LeCheminant AN (2001) Enriched Archean lithospheric mantle beneath western Churchill Province tapped during Paleoproterozoic orogenesis. Geology 29:827–830

Fahrig WF, Christie KW, Eade KE, Tella S (1984) Paleomagnetism of the Tulemalu dykes, Northwest Territories, Canada. Can J Earth Sci 21:544–553

Flowers RM (2005) Stabilization, reactivation, and exhumation of cratonic lithosphere: a view from the lower crust, East Lake Athabasca region, western Canadian Shield. PhD Thesis, Massachusetts Institute of Technology, 228 pp

Flowers RM, Mahan KH, Bowring SA, Williams ML, Pringle MS, Hodges KV (2006) Multistage exhumation and juxtaposition of lower continental crust in the western Canadian Shield: linking high-resolution U–Pb and $^{40}Ar/^{39}Ar$ thermochronometry with *P–T–D* paths. Tectonics (in review)

Goodacre AK, Grieve RAF, Halpenny JF, Sharpton VL, (1987) Horizontal gradient of the Bouguer gravity anomaly map of Canada. Canadian Geophysical Atlas, Map 5

Gordon TM (1988) Precambrian geology of the Daly Bay area, District of Keewatin. Geol Surv Can Mem 422:21

Hanmer S (1994) Geology, East Athabasca mylonite triangle, Saskatchewan. Geol Surv Can Map, 1859A

Hanmer S (1997) Geology of the striding-Athabasca mylonite zone, northern Saskatchewan and southeastern District of Mackenzie, Northwest Territories. Geol Surv Can Bull 501:92

Hanmer S, Williams M (2001) Targeted fieldwork in the Daly Bay Complex, Hudson Bay, Nunavut. Geol Surv Can Curr Res, 2001-C15

Hanmer S, Williams M, Kopf C (1995a) Modest movements, spectacular fabrics in an intracontinental deep-crustal strike-slip fault: striding-Athabasca mylonite zone, NW Canadian Shield. J Struct Geol 17:493–507

Hanmer S, Williams M, Kopf C (1995b) Striding-Athabasca mylonite zone: implications for the Archean and Early Proterozoic tectonics of the western Canadian Shield. Can J Earth Sci 332:178–196

Hanson GN, Catanzaro EJ, Anderson DH (1971) U–Pb ages for sphene in a contact metamorphic zone. Earth Planet Sci Lett 12:231–237

Hartel THD, Pattison DRM (1996) Genesis of the Kapuskasing (Ontario) migmatitic mafic granulites by dehydration of melting of amphibolite: the importance of quartz to reaction progress. J Metamorph Geol 14:591–611

Hoffman PF (1988) United Plates of America, the birth of a craton: Early Proterozoic assembly and growth of Laurentia. Annu Rev Earth Planet Sci Lett 16:545–603

Jaffey AH, Flynn KF, Glendenin LE, Bentley WC, Essling AM (1971) Precision measurements of half-lives and specific activities of ^{235}U and ^{238}U. Phys Rev C4:1889–1906

Kopf C (1999) Deformation, metamorphism, and magmatism in the East Athabasca mylonite triangle, northern Saskatchewan: implications for the Archean and Early Proterozoic crustal structure of the Canadian Shield. PhD dissertation Thesis, University of Massachusetts-Amherst, 208 pp

Krikorian L (2002) Geology of the Wholdaia Lake segment of the Snowbird Tectonic Zone, Northwest Territories (Nunavut): a view of the deep crust during assembly and stabilization of the Laurentian craton. Msc Thesis, University of Massachusetts-Amherst, 90 pp

Krogh TE (1973) A low contamination method for hydrothermal decomposition of zircon and extraction of U and Pb for isotopic age determinations. Geochim Cosmochim Acta 37:485–494

Krogh TE (1982) Improved accuracy of U–Pb zircon ages by the creation of more concordant systems using an abrasion technique. Geochim Cosmochim Acta 46:637–649

Lambert IB, Wyllie PJ (1974) Melting of tonalite and crystallization of andesite liquid with excess water to 30 kilobars. J Geol 82:88–97

Lewry JF, Sibbald TII (1980) Thermotectonic evolution of the Churchill Province in northern Saskatchewan. Tectonophysics 68:5–82

Ludwig KR (1980) Calculation of uncertainties of U–Pb isotope data. Earth Planet Sci Lett 46:212–220

MacDonald R (1980) New edition of the geological map of Saskatchewan, Precambrian shield area. In: Summary of investigations, Saskatchewan Geological Survey, Regina, pp 19–21

Mahan KH, Williams ML (2005) Reconstruction of a large deep-crustal exposure: implications for the Snowbird tectonic zone and early growth of Laurentia. Geology 33:385–388

Mahan KH, Williams ML, Baldwin JA (2003) Contractional uplift of deep crustal rocks along the Legs Lake shear zone, western Churchill Province, Canadian Shield. Can J Earth Sci 40:1085–1110

Mahan KH, Goncalves P, Williams ML, Jercinovic MJ (2006) Dating metamorphic reactions and fluid flow: application to exhumation of high-P granulites in a crustal-scale shear zone, western Canadian Shield. J Met Geol (in press)

Mills A, Berman RG, Hanmer SK, Davis W (2000) New insights into the tectonometamorphic history of the Uvauk complex, Nunavut. GeoCanada 2000 CD-ROM, Geological Association Canada, Abstract 733

Patino Douce AE (2005) Vapor-absent melting of tonalite at 15–32 kbar. J Petrol 46:275–290

Patino Douce AE, Beard JS (1995) Dehydration-melting of biotite gneiss and quartz amphibolite from 3 to 15 kbar. J Petrol 36:707–738

Petford N, Gallagher K (2001) Partial melting of mafic (amphibolitic) lower crust by periodic influx of basaltic magma Earth Planet Sci Lett 193:483–499

Rapp RP, Watson EB (1995) Dehydration melting of metabasalt at 8–32 kbar: implications for continental growth and crust-mantle recycling. J Petrol 36:891–931

Rapp RP, Watson EB, Miller CF (1991) Partial melting of amphibolite/eclogite and the origin of Archean trondhjemites and tonalities. Precambrian Res 51:1–25

Ross GM, Milkereit B, Eaton D, White D, Kanasewich ER, Burianyk MJA (1995) Paleoproterozoic collisional orogen beneath the western Canada sedimentary basin imaged by Lithoprobe crustal seismic reflection data. Geology 23:195–199

Ross GM, Eaton DW, Boerner DE, Miles W (2000) Tectonic entrapment and its role in the evolution of continental lithosphere: an example from the Precambrian of western Canada. Tectonics 19:116–134

Rushmer T (1991) Partial melting of two amphibolites: contrasting experimental results under fluid-absent conditions. Contrib Mineral Petrol 107:41–59

Sanborn-Barrie M, Carr SD, Theriault R (2001) Geochronological constraints on metamorphism, magmatism and exhumation of deep-crustal rocks of the Kramanituar Complex, with implications for the Paleoproterozoic evolution of the Archean western Churchill Province, Canada. Contrib Mineral Petrol 141:592–612

Sandeman H, Cousens B, Hemmingway D (2003) Continental tholeiitic mafic rocksof the Paleoproterozoic Hurwitz Geoup, Central Hearne sub-domain Nunavut: insight into the evolution of the Hearne sub-continental lithosphere. Can J Earth Sci 40:1219–1237

Schmidt MW (1993) Phase-relations and compositions in tonalite as a function of pressure an experimental study at 650°C. Am J Sci 293:1011–1060

Skjerlie KP, Johnston AD (1993) Fluid absent melting of a layered crustal protolith—implications for the generation of anatectic granites. Contrib Mineral Petrol 114:365–378

Skjerlie KP, Johnston AD (1996) Vapour-absent melting from 10 to 20 kbar of crustal rocks that contrain multiple hydrous phases: implications for anatexis in the deep to very deep continental crus and active continental margins. J Petrol 37:661–691

Snoeyenbos DR, Williams ML, Hanmer S (1995) Archean high-pressure metamorphism in the western Canadian Shield. Eur J Min 7:1251–1272

Springer W, Seck HA (1997) Partial fusion of basic granulites at 5 to 15 kbar: implications for the origin of TTG magmas. Contrib Mineral Petrol 127:30–45

Stacey JC, Kramers JD (1975) Approximation of terrestrial lead isotope evolution by a two-stage model. Earth Planet Sci Lett 26:207–221

Sun SS, McDonough WF (1989) Chemical and isotopic systematics of oceanic basalts: implications for mantle composition and processes. In: Saunders AD, Norry MJ (eds) Magmatism in oceanic basins. Geological Society Special Publication, London, pp 313–345

Tella S, Eade KE (1986) Occurrence and possible tectonic significance of high-pressure granulite fragments in the Tulemalu fault zone, District of Keewatin, N.W.T., Canada. Can J Earth Sci 23:1950–1962

Vavra G, Schmid R, Gebauer D (1999) Internal morphology, habit and U–Th–Pb microanalysis of amphibolite-to-granulite facies zircons: geochronology of the Ivrea Zone (Southern Alps). Contrib Mineral Petrol 134:380–404

Williams ML, Hanmer S (2005) Structural and metamorphic processes in the lower crust: evidence from an isobarically cooled terrane, the East Athabasca mylonite triangle. In: Brown M, Rushmer T (eds) Evolution and differentiation of the continental crust. Cambridge University Press, Cambridge, pp 232–268

Williams ML, Hanmer S, Kopf C, Darrach M (1995) Syntectonic generation and segregation of tonalitic melts from amphibolite dikes in the lower crust, Striding-Athabasca mylonite zone, northern Saskatchewan. J Geophys Res 100:15717–15734

Williams ML, Mellis EA, Kopf C, Hanmer S (2000) Microstructural Tectonometamorphic processes and the development of gneissic layering: a mechanism for metamorphic segregation. J Metamorph Geol 18:41–57

Wolf MB, Wyllie PJ (1993) Garnet growth during amphibolite anatexis: implications of a garnetiferous restite. J Geol 101:357–373

Wolf MB, Wyllie PJ (1994) Dehydration-melting of amphibolite at 10 kbar: the effects of temperature and time. Contrib Mineral Petrol 115:369–383

Wolf MB, Wyllie PJ (1995) Liquid segregation parameters from amphibolite dehydration melting experiments. J Geophys Res 100:15611–15621